1973

Experimental analysis of v-belt tensile loads

John Mark Wiesehan

Department:

EXPERIMENTAL ANALYSIS OF V-BELT TENSILE LOADS

By

John Mark Wiesehan, 1951 -

A THESIS

Presented to the Faculty of the Graduate School of the

UNIVERSITY OF MISSOURI - ROLLA

In Partial Fulfillment of the Requirements for the Degree

MASTER OF SCIENCE IN MECHANICAL ENGINEERING

1973

Approved By

Donald L. Grimm (Advisor) Clark R. Barker

Harold Wm. Keith

Notice to individuals who would reproduce
this thesis:

Total number of pages is 107. Thesis contains
an added page numbered 30a.

ABSTRACT

An experimental investigation was conducted to determine the magnitude of v-belt stresses in automotive drive situations. A constant tension belt test apparatus was designed and fabricated using a variable speed cradled D.C. motor for power and two automotive alternators for absorption.

Free span stresses on the dynamic torque loaded belt drive were determined from the equations governing a pivoted drive system. Centrifugal stress was determined by a theoretical analysis of belt motion. Bending stresses were obtained from a static test employing strain gages mounted on the top of belts with exposed cord layers. The variation in load stress around the pulleys in a dynamic torque loaded drive was to be determined by taking time synchronized photographs of a marked belt section and measuring strain from enlarged photographic negatives. The time synchronization of high speed close-up photography was accomplished during this study, but the capability of making measurements from photographic data was not perfected. Insight gained from this work led to the advancement of ideas which may allow photographic determination of belt strain in a future study. A magnetic pickoff and timer system also failed to indicate the magnitude of dynamic belt strains. In order to complete the present analysis, the Hornung analytical solution for tensions around torque loaded pulleys was employed in a digital simulation program. A matrix of computer runs was made for the range of drive parameters studied. Finally, power losses in belt

drives were experimentally obtained in order to determine the design acceptability of the drive situations tested.

Superposition of bending, centrifugal and load tensions led to the conclusion that bending stress is by far the largest stress factor to be considered in automotive v-belt drives. The fact that small changes in load stress cause noticeable changes in belt fatigue life must be attributed to the creep, slip, and heat generation phenomena which accompany torque transmission.

ACKNOWLEDGEMENTS

The author wishes to express thanks to Dr. D. L. Cronin for his guidance during this study. Appreciation is extended to the Mechanical Engineering Department for teaching and research assistantships during the 1972-73 academic year. The author is also grateful to the Ford Motor Company for financial support during the summer of 1973 and to the Dayco Corporation for furnishing production v-belts, specially fabricated v-belts, test pulleys, and belt materials' parameters used in this study. Appreciation is expressed especially toward Dr. Larry Oliver and Mr. Clyde Johnson of the Dayco Corporation for their experienced technical counsel and aid in establishing meaningful experimental goals for this study.

TABLE OF CONTENTS

Table of Contents (continued)

LIST OF SYMBOLS

a — Distance from pivot axis to center of driven pulley shaft in a pivoted drive system (in.).

A — Cross sectional area of a single v-belt cord ($in.^2$).

D — Outside diameter of a v-belt cord (in.).

e — Radial eccentricity of a point in question with respect to the neutral axis of a v-belt bent around a pulley sheave. e is positive radially outward from the neutral axis (in.).

e_{top} — Radial eccentricity of the top of the cord layer in a v-belt bent around a pulley sheave (in.).

e_z — Radial eccentricity of the elevation of zero stress in a v-belt preloaded and bent around a pulley sheave (in.).

$\bar{e}_r$ — Radial unit vector, positive outward radially.

$\bar{e}_t$ — Tangential unit vector, positive in the direction of belt motion.

$\bar{e}_a$ — Axial unit vector, positive in the direction $(\bar{e}_r \times \bar{e}_t)$, directed along the shaft axis.

$\bar{e}_x$ — Unit vector equivalent to $\bar{e}_t$ at $\theta = 0$.

$\bar{e}_y$ — Unit vector equivalent to $\bar{e}_r$ at $\theta = 0$.

E_c — Elastic modulus of v-belt cords in compression $\left(\frac{lbf.}{in.^2} / \frac{in.}{in.}\right)$.

E_t — Elastic modulus of v-belt cords in tension $\left(\frac{lbf.}{in.^2} / \frac{in.}{in.}\right)$.

FR_R — Torque exerted on driver pulley; motor torque (lbf. ft.).

FR_N — Torque exerted on driven pulley; load torque (lbf. ft.).

F_c — Centrifugal force on an element of belt $rd\theta$ units long moving through the pulley sheave (lbf.).

F_{c_x} — Component of F_c in the $\bar{e}_x$ direction (lbf.).

F_1 The sum of load tension and centrifugal tension in the slack span of a belt drive (lbf.)

F_2 The sum of load tension and centrifugal tension in the tight span of a belt drive (lbf.).

g Gravitational constant; 32.2 $\left(\frac{\text{lbm. ft.}}{\text{lbf. sec.}^2}\right)$.

l Distance from pivot axis to line of loading force on a pivoted drive (in.).

M_a Axial elastic belt modulus per inch of belt $\left(\frac{\text{lbf.}}{\text{in.}} / \frac{\text{in.}}{\text{in.}}\right)$.

M_{cord} Tangential elastic modulus of a single v-belt cord $\left(\text{lbf.}/\frac{\text{in.}}{\text{in.}}\right)$.

M_t Tangential elastic modulus of an entire v-belt $\left(\text{lbf.}/\frac{\text{in.}}{\text{in.}}\right)$.

n Number of cords in the cord layer of a v-belt.

N_N Angular speed of driven pulley (RPM).

N_R Angular speed of driver pulley (RPM).

P Loading force in a constant tension drive (lbf.).

r Radius of the neutral axis of the belt in bending equations. Radius of centroid of belt mass in centrifugal stress equations.

r_N Pitch radius of driven pulley (in.).

r_R Pitch radius of driver pulley (in.).

s_E Elastic creep or change in strain state in a belt due to change in load tension $\left(\frac{\text{in.}}{\text{in.}}\right)$.

s_N Driven pulley run-on slip. (A ratio limited by 0 and 1.)

s_R Driver pulley run-on slip. (A ratio limited by 0 and 1.)

s_T Transmission ratio slip. (A ratio limited by 0 and 1.)

s_{tot} Total fraction of power input into a belt drive which is lost between driver and driven pulleys. (A ratio limited by 0 and 1.).

S Radius of the top of the cords in a v-belt with respect to the pulley axis (in.).

$T(\theta)$ Load tension in a v-belt at position θ in the pulley sheave (lbf.).

T_1 Tight span load tension in a torque loaded v-belt drive (lbf.).

T_2 Slack span load tension in a torque loaded v-belt drive (lbf.).

T_c Span tension component due to centrifugal force acting on the portion of belt in the pulley sheaves (lbf.).

v Linear velocity of v-belt $\left(\frac{\text{ft.}}{\text{sec.}}\right)$.

v_1 Linear velocity of the tight span of a v-belt drive $\left(\frac{\text{ft.}}{\text{sec.}}\right)$.

v_2 Linear velocity of the slack span of a v-belt drive $\left(\frac{\text{ft.}}{\text{sec.}}\right)$.

δe_{top} Error involved in computation of e_{top} (in.).

δe_z Error involved in computation of e_z (in.).

$\Delta\varepsilon_{\substack{max \\ load}}$ Change in cord strain resulting from change in load tension from T_1 to T_2 $\left(\frac{\text{in.}}{\text{in.}}\right)$.

ε_B General expression for bending strain $\left(\frac{\text{in.}}{\text{in.}}\right)$.

$\varepsilon_{B_{top}}$ Bending strain in top fibers of cord layer $\left(\frac{\text{in.}}{\text{in.}}\right)$.

ε_P Cord strain resulting from preload tension $\left(\frac{\text{in.}}{\text{in.}}\right)$.

ε_{P_i} Strain indicator reading for cord mounted strain gage at center of free span $\left(\frac{\text{in.}}{\text{in.}}\right)$.

ε_{tot} The sum of bending and load strain on the top fibers of the cord layer at a point in the wrap angle $\left(\frac{\text{in.}}{\text{in.}}\right)$.

ε_{tot_i} Strain indicator reading for cord mounted strain gage positioned in the wrap angle $\left(\frac{\text{in.}}{\text{in.}}\right)$.

ε_u Cord strain on the bottom fibers of the cord layer $\left(\frac{\text{in.}}{\text{in.}}\right)$.

θ_N Wrap angle on driven pulley. $\theta_N = 0$ where the belt enters the driven pulley sheave (radians).

θ_R Wrap angle on driver pulley. θ_R = 0 where the belt enters the driver pulley sheave (radians).

ρ Mass of belt per unit length (lbm./ft.) .

σ_{B_C} Compressive bending stress $\left(\frac{\text{lbf.}}{\text{in.}^2}\right)$.

σ_{B_t} Tensile bending stress $\left(\frac{\text{lbf.}}{\text{in.}^2}\right)$.

σ_{cord} Total cord stress at any point in the cord layer composed of load, centrifugal and bending components $\left(\frac{\text{lbf.}}{\text{in.}^2}\right)$.

$\sigma_{B_{top}}$ Bending stress on the top fibers of the cord layer $\left(\frac{\text{lbf.}}{\text{in.}^2}\right)$.

σ_P Cord stress resulting from preload tension $\left(\frac{\text{lbf.}}{\text{in.}^2}\right)$.

σ_{tot} The sum of bending and load stress on the top fibers of the cord layer at a point in the wrap angle $\left(\frac{\text{lbf.}}{\text{in.}^2}\right)$.

ψ Traction Coefficient; $(T_1 - T_2)/(T_1 + T_2)$.

ψ_o The value of ψ at which power loss becomes a non-linear function of ψ.

ω The magnitude of the angular velocity of a pulley $\left(\frac{\text{rad.}}{\text{sec.}}\right)$

ω_N The magnitude of the angular velocity of a driven pulley $\left(\frac{\text{rad.}}{\text{sec.}}\right)$.

ω_R The magnitude of the angular velocity of a driver pulley $\left(\frac{\text{rad.}}{\text{sec.}}\right)$.

LIST OF ILLUSTRATIONS

List of Illustrations (continued)

List of Illustrations (continued)

I. INTRODUCTION

The v-belts used to drive auxiliary automotive equipment such as fans, pumps, and compressors have evolved from a line of flexible machine elements. Early in the machine age, flat leather or woven fabric belts were used to transmit power to machines from a centrally located prime mover. Following the commercial availability of textile fabric-reinforced rubber, the first v-belt was patented in 1917.

The design of modern v-belts of the type shown in Figure 1.1 is based on the results of empirical optimizations. It is at once clear that the vee-shape of the belt causes it to wedge in a v-groove pulley when acted upon by the tensions in the free spans of belt between the pulleys. This wedging action reduces slippage and provides for more efficient torque transmission than could be achieved with a flat belt. The commonly used 36 degree included angle cross section produces what is generally considered to be a balance of good efficiency and reasonable belt life. Belts with larger included v-angles are known for longer life because of the low amount of wedging frictional scrub between the belt and pulley. Belts with smaller v-angles are known for high wedging forces and hence high torque transmission capability, but for short life because of the detrimental effects of the wedging friction. Since the purpose of this study is to examine automotive accessory drive belts, only the 36 degree included angle cross section belts have been treated.

More specifically, the v-belts used in this study were die-cut belts manufactured by the Dayco Corporation for the automobile

industry. The construction of these belts involves the application of successive layers of material around a tubular mandrel several feet long. The resulting sleeve is cured and then rotated on a lathe-like cutting machine and sliced into several dozen belts. The layered construction of the resulting die-cut belts used in this study is illustrated in Figure 1.1. At the bottom of the belt there are multiple layers of fabric impregnated rubber (Figure 1.1.a) which handle the comparatively large compressive forces encountered as the belt travels around the pulley sheave. This construction provides a wear resistant surface on the lower sides of the belt. Above the fabric and rubber section is a layer of either soft rubber or a composite of rubber and chopped fibers (Figure 1.1.c). This layer provides the flexibility required for the cord layer to conform to small pulley radii and serves to transmit high bending shear stresses near the neutral axis to the lower fabric and rubber layer. Above this soft rubber section is a layer of cords (Figure 1.1.b), the chief tensile load carrying constituents of the belt. Cord is wound helically on the belt sleeve during the manufacturing process so that what appears to be a set of cords is actually one cord. The cord layer, now commonly made of synthetic fibers such as Dacron Polyester and fiberglass has been found to carry approximately 96 percent of the belt tensile load [10]. Hence, the cord layer is the most important element to consider in a study of v-belt tensile loads. Above the cord layer is another soft layer of rubber (Figure 1.1.c) which again contributes to the flexibility of the belt and withstands the high bending shear strain near the neutral axis. The belt is

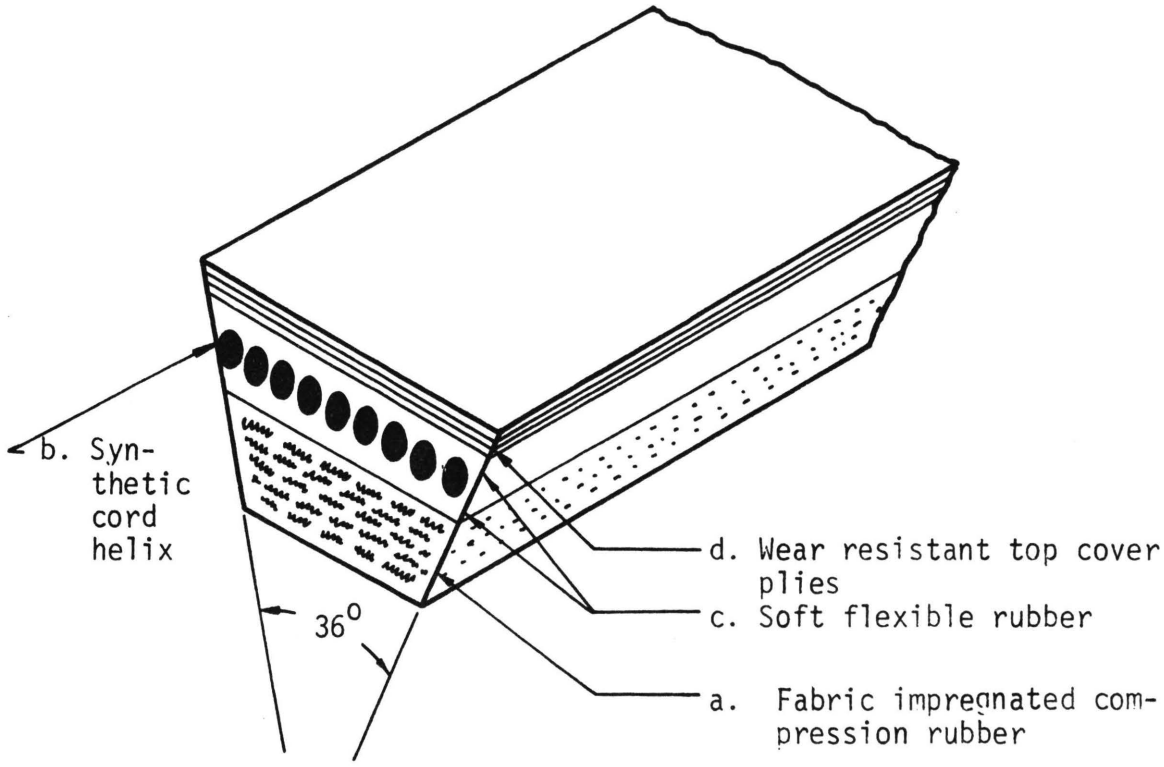

Figure 1.1. Built-up Cross Section of a Die-cut V-belt

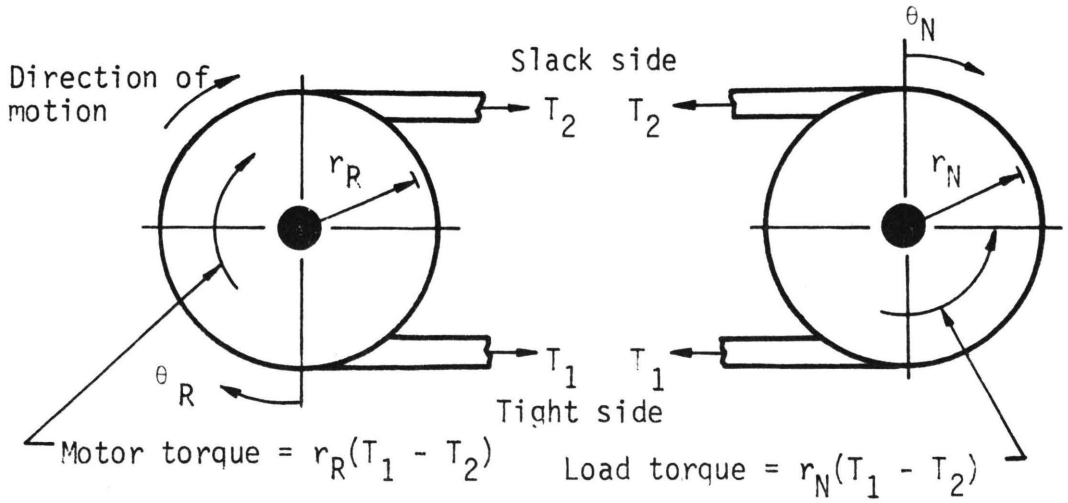

Figure 1.2. Tensions and Torques on a Two Pulley V-belt Drive

then topped with several plies of tough rubberized fabric (Figure 1.1.d) that protect the cord layer from abrasions that may initiate unwrap or fracture.

Two special features sometimes used on v-belts and not studied in this report are a cogged inner side and a uniform covering over the belt of a highly wear resistant composite rubber and fabric. Excessive frictional scrub due to high compression and buckling of the lower belt fibers is eliminated by the cogged configuration. This increases belt life where small diameter pulleys are used. The wear resistant composite covering is employed to prolong belt life where dust or sand in the operating environment may cause excessive wear between the pulley sheave and the belt.

Mathematical determination of v-belt drive loads produces a host of problems not only because of the complex nature of belt construction, but also because of the three dimensional rotating force system acting on the belt as it travels around the pulley in contact with the wedge-shaped walls or sheave of the pulley. Qualitatively, these forces may be considered as shown in Figures 1.2 and 1.3. Acting as a flexible drive link, the v-belt must transmit a torque from the driver to the driven pulley. A free body diagram as shown in Figure 1.2 cut anywhere in the free spans of a two pulley drive exposes the fact that there must be a tension difference in order to transmit this torque. This tension difference multiplied by the pitch radius of the pulley must equal the torque transmitted. The pitch radius is defined as the pulley radius where the linear velocity of an untorqued belt system is equal to the tangential pulley velocity. Since the belt is an elastic

element, it must contract as it passes over the driver pulley and stretch as it passes over the driven pulley because the two stress levels in the free spans specify two different strain states. This deformation in the direction of motion related to the transmission of torque is commonly known as elastic belt creep and is present in all torque loaded belt drives. Deformation is not only tangential, however, because the wedging of the belt in the pulley sheave also causes deformations in the axial and radial directions as shown in Figure 1.3. The fact that the belt is bent around circular pulleys in its path of motion introduces bending stresses and centrifugal forces into a complete belt analysis. Lastly, since the v-belt transmits torque through wedging friction, it is subject to frictional forces and slippage in the plane of the pulley sheave, and wedging forces in the plane normal to the sheave surfaces.

The overall purpose of this thesis is to provide an experimental analysis of v-belt force and stress systems and belt motion relative to the pulley. The analysis presented here, it is hoped, will contribute to the improvement of existing belt drive design criteria and to the more accurate specification of the cyclic stresses used in belt fatigue equations. More specifically, the purpose of this study is to determine the effects of change in torque, pulley size, preload, and belt speed on the stresses encountered during a cycle of operation for a two pulley drive system. The force and stress analysis includes calculation of static tensions, load carrying tensions, centrifugal tensions, and bending stress by experimental or analytical methods. The end product is a superposition of all these forces and stresses

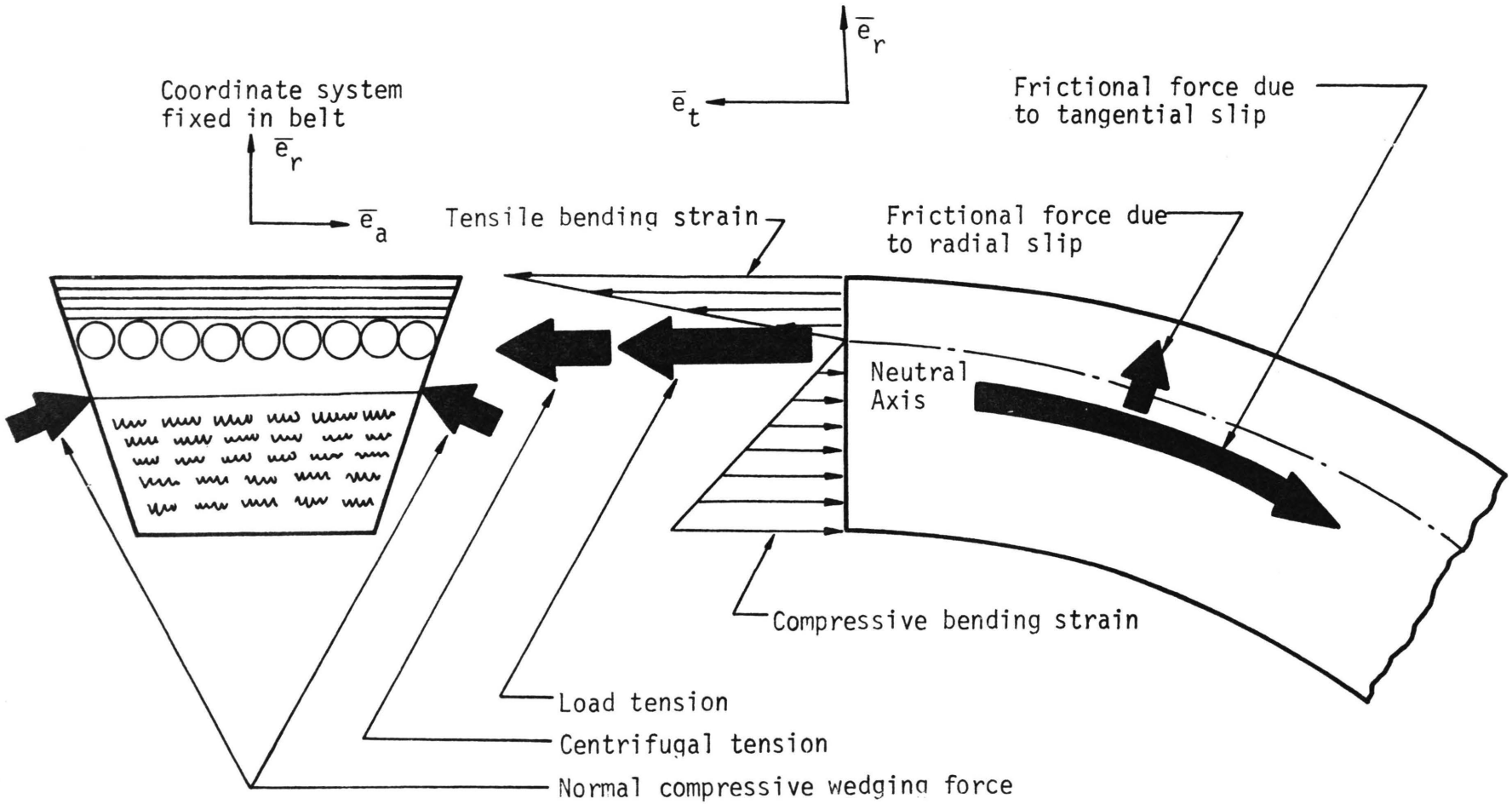

Figure 1.3. Qualitative Analysis of Forces on a Segment of Belt Moving Through the Pulley Sheave

to yield a total picture of belt stress during a cycle of operation. An order of magnitude analysis for all these forces and stresses was accomplished for automotive type drives in order to show the interactions between tensions for differing drive parameters and to arrange a hierarchy of stress component magnitudes for the reader. Finally, based on experience gained with several belt stress measuring devices, recommendations are given for a precision test apparatus for complete experimental dynamic stress analysis of v-belt drives.

II. REVIEW OF LITERATURE

There are several basic problem areas addressed by the literature on v-belts. First, experimental and analytical work considers stress analysis of belts and the generalized effects of torque load, preload, speed, and system geometry on the stresses encountered. Next, consideration is given to the interaction of the torque transmission process with radial and tangential relative motion between the belt and pulley sheave. This problem is dealt with on a continuum basis in some analyses which consider the variation in wedging forces, belt-sheave friction coefficients and belt elasticity, and the effect of these factors on belt motion relative to the pulley. Power losses and efficiencies in belt drives are most often calculated from gross quantities such as tight and slack span tensions, belt and pulley velocities, and transmission ratios due to the change in belt pitch radius. The sources of heat generation and belt vibration are also explored in the literature in an attempt to minimize these harmful side-effects on a dynamic power-transmitting belt drive. The culmination of all areas of study is the use of stress, relative motion, heat generation, and vibration technology to determine design criteria and fatigue life for belt drives.

Constant tension v-belt drive systems such as the pivoted or slide mounted drives (Figures 3.1, 3.2) which allow the static calculation of free span tensions are commonly discussed in the literature [7, 9, 12]. Hornung, Marco, and Starkey [7, 8] have done an analysis of belt geometry and tension variation in a locked centers drive. This locked centers analysis, however, requires experimental determination of one

parameter for every type of belt used and a trial and error iteration of the final solution for the tight and slack span tensions. The determination of centrifugal forces and their effect on span tension is derived from a generalized analysis by Hornung in Reference 7 .

The next important consideration in v-belt analysis is that of defining the equations of belt motion in terms of force and stress summations in the three orthogonal directions and variations of these with respect to belt position in the pulley sheaves and free spans. Since v-pulleys are made so that the bottom of the belt never touches the bottom of the pulley groove, both radial and tangential motion must be considered. Presently, every v-belt analysis contains several simplifications in its derivation of the equations of motion. The Hornung solution 7 for the variation of load tension and belt motion relative to the pulley considers unloading of the working tension after the belt is completely seated in the v-groove. Hornung also models the belt as a thin elastic ribbon so that bending effects and radial distribution of wedging stress may be uncoupled from the equations of motion. After simplification, Hornung offers four ordinary differential equations involving four independent variables and one dependent variable, θ, the angular position of the belt on the pulley sheave. Independent variables are the tangential belt tension, a tangential motion coordinate, an angle relating radial and tangential motion, and a distributed force per unit length which is the resultant of the wedging stress. The Hornung equations have been programmed as a digital simulation so that given initial conditions, values of the variables may be calculated over the angle of contact between belt and pulley.

In addition to Hornung's original analysis [7], Marco, Starkey, and Hornung [10] have done a fatigue analysis on the v-belt cord layer which includes the superposition of a bending stress term on the sum of load carrying and centrifugal stress components endured by the belt in the pulley sheave.

Other theoretical analyses which consider the interaction between load stress and shear stress due to torque transfer have been performed by Martynov [11] and Gerbert [5]. Martynov writes the interaction between shear and load stress in terms of Laplace's equation. He then approximates the solution for belt displacement relative to the pulley as the first term of the series solution to the equation. The sinusoidal component of the solution is assigned to belt displacement in the axial direction and the hyperbolic component is assigned to relative displacement in the tangential direction. Belt shear and tangential belt stresses are obtained by closed form integrals involving the displacement solution. The arc of contact between belt and pulley is divided into an adhesion zone and a sliding zone. The length of these zones is also determinable given wedging friction coefficients and span tensions. Martynov continues with the analysis of the factors involved in belt transmission power losses similar to those described in Section III. He concludes by comparing an analytical analysis of power loss components with an experimental analysis of total power loss.

Gerbert [5] continues Martynov's theoretical work by changing the Martynov Laplacian to cylindrical coordinates and writing infinite series solutions for belt displacement relative to the pulleys.

Gerbert's cylindrical coordinate system allows the calculation of cord stress distribution in the axial direction. Gerbert verifies his theory of axial stress distribution with a static experimental test. Gerbert [6] has also attacked the problem of radial stress distribution and radial displacement of the v-belt in the pulley sheave and has produced analytical results with a finite element analysis. This approach takes into account the variation of material parameters due to the composite nature of belt construction.

Power losses in multiple-pulley belt drives are examined by Garrett [4], but his analysis considers only what is known as elastic creep for computation of power losses. Belt power losses due to run-on slip and elastic creep are examined with respect to traction coefficients in a paper by Virabov [16]. Pronin and Shmelev [13] examine these same loss components plus bending, aerodynamic, and axial compression effects which reduce belt efficiency. In this paper the loss components are separated by an experimental analysis involving flat belt and v-belt drives under loaded and unloaded conditions. Relative motion of a v-belt with respect to driver and driven pulleys was also examined by Meyer [12]. His analysis consisted of mounting a movie camera on a v-pulley and focusing it on the belt through a small hole in the side of the pulley. Experimental determination of relative motion between the belt and pulley was accomplished by Meyer's analysis, but the bulk and fragility of the camera and lighting system required that low speeds and very large pulleys be used.

A theory of constant mass in belt drives has been advanced by Virabov [17] where local belt stresses are shown to be related to

local belt velocities. This theory considers the belt to be much like a fluid flowing at a constant mass rate. It may be recognized that the rate of belt mass traveling into a pulley must equal the rate of mass departing for steady state operation. This concept may be extended to any local control volume around the pulleys. Constant mass theory requires that the product of the belt mass per unit length and the belt velocity be constant in a given drive situation. Also, the percentage change in mass per unit length is set equal to the negative of the change in strain. The combination of these two concepts allows the relating of stress to velocity in a single equation.

Several other aspects of v-belt transmission systems have been examined in the past. A lateral vibration analysis has been completed by Doyle and Hornung [3] while research is presently continuing on the determination of lateral and torsional eigenvalues in a fixed centers drive. Experimental frequency response analysis of the axial properties of v-belts has been accomplished by Chin-Heng [2] and Bowen [1]. The source of heat generation and the heat transmission capabilities of v-belt drives has been studied by Shade [14] for unloaded drives and by Upchurch [15] for torque loaded drives. Correlation between analytical conduction-convection-generation heat transfer models and experimentally measured heat transfer was generally not very strong because of the poor definition of frictional and hysteretic heat generation effects.

The ultimate goal of all v-belt analyses is to add to or alter existing belt fatigue theory and drive design criteria. Cord fatigue

equations are advanced by Marco, Starkey, and Hornung [10]. Nomographs of belt fatigue with respect to drive parameters are given by Johnson and Hornung [9] while the general theory of cumulative damage is discussed by Hornung [7]. Fatigue life information and drive design criteria are discussed extensively by Worley [18].

Finally, belt analyses have considered stresses, stress distribution, power losses, drive geometries, heat transfer, and vibration effects as the governing factors in drive design and belt fatigue theory. Fatigue analyses have attempted to correlate all these factors with years of fatigue data in order to more accurately specify belt designs and design life of belt drives.

Substantial progress has been made toward the solution of problems of direct engineering interest: How long will a given system survive repetitions of a given loading cycle? How must a system be designed to survive repetitions of a given loading cycle for so many hours? Representatives from industry have expressed concern, however, that many questions still require answers before a fully developed fatigue theory for v-belts can be regarded as complete. These questions relate in part to the lack of experimental data supporting assumptions made in the theoretical studies discussed above. The study reported in the following sections addresses one of the areas where industrial representatives have identified a need for experimental data.

III. MATHEMATICAL DEVELOPMENT

Two basic types of v-belt drives are presently employed. They are the constant tension drive and the fixed centers drive shown in Figures 3.1, 3.2, and 3.3. The automotive industry generally utilizes the fixed centers drive while the constant tension drive is often used on stationary equipment. For experimental purposes, the constant tension drive has an advantage over the fixed centers system in that the free span tensions in the belt can be calculated from static analysis. Determination of stress and tension variations in the belt as it passes through a sheave may then be made using the free span tensions as a relative dynamic basis for calibration of the instrumentation used.

An analysis of the free span tensions in a fixed-centers drive was made by Hornung, Marco, and Starkey [8] and is referenced in Section II. Experimental determination of a constant parameter, K_B, and trial and error iteration for the free span tensions are the main disadvantages of this method.

The constant tension drive configuration was chosen for the present investigation. The governing equations for span tensions in a constant tension pivoted drive may be easily derived. For the system represented in Figure 3.2, the governing equations for the free span tensions are

$$T_1 - T_2 = \frac{FR_R}{r_R} \tag{3.1}$$

$$(a - r_N)T_1 + (a + r_N)T_2 = Pl \tag{3.2}$$

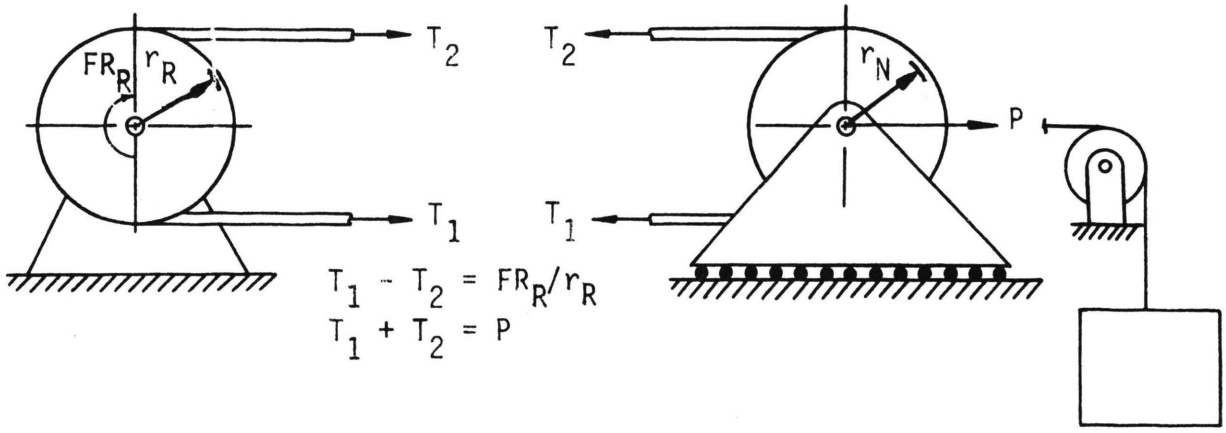

Figure 3.1. Slide Mounted Constant Tension Drive

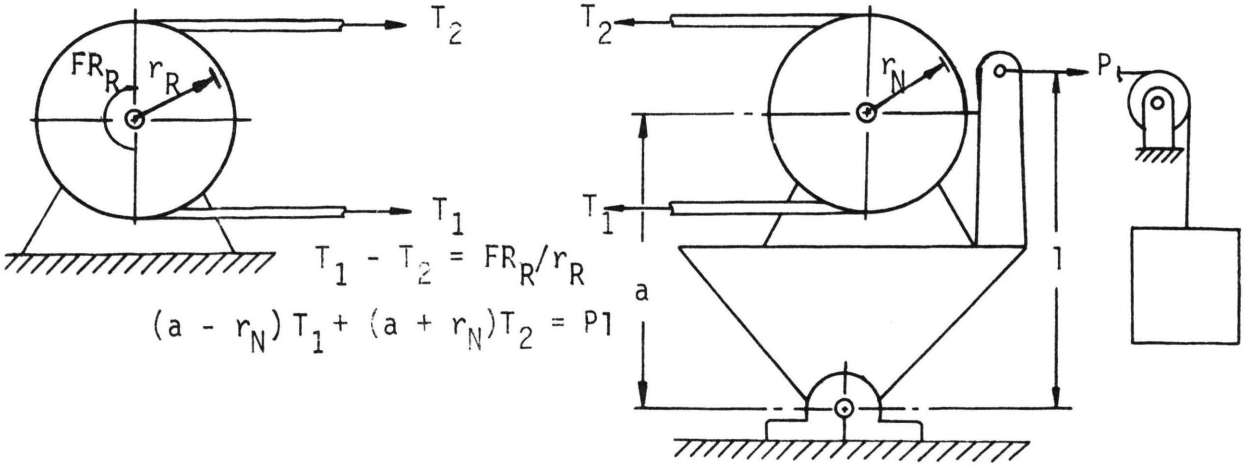

Figure 3.2. Pivot Mounted Constant Tension Drive

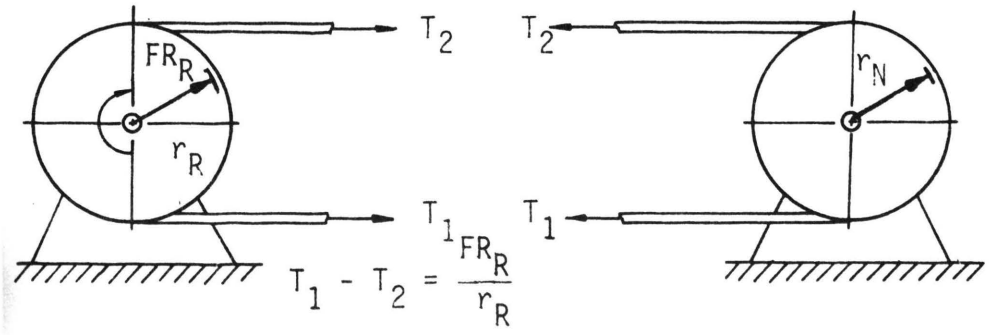

Figure 3.3. Fixed (or Locked) Centers Drive

where l, a, and R are defined on Figure 3.2, and FR_R is the input motor torque which can be determined by measuring the torque required to restrain a cradle-mounted electric motor or by using strain gages and slip rings on the input shaft. P may be determined from a force transducer in line with the preloading force. Hence, T_1 and T_2 are the only unknowns in Equations 3.1 and 3.2 and simultaneous solution is possible. For driver and driven pulleys of the same diameter, r_N r_R and the solutions are

$$T_1 = \frac{1}{2}\left[\frac{Pl + FR_R}{a} + \frac{FR_R}{r_R}\right] \tag{3.3}$$

$$T_2 = \frac{1}{2}\left[\frac{Pl + FR_R}{a} - \frac{FR_R}{r_R}\right] \tag{3.4}$$

T_1 will be referred to as the tight side tension and T_2 as the slack side tension in following references ($T_1 \geq T_2$).

These tensions do not include the centrifugal force effect. This effect may be developed by considering the mass of belt in contact with the pulley sheave. The centrifugal force on an element of length $rd\theta$ shown in Figure 3.4 is

$$F_c = \frac{\rho}{g} r\omega^2 (rd\theta) \tag{3.5}$$

where ρ is the mass per unit length of the belt, r is the centroid of the belt, ω is the angular velocity of the belt, and g is the gravitational constant. The x-component of this force is

$$F_{c_x} = \frac{\rho}{g} r\omega^2 \sin\theta\ (rd\theta) = \frac{\rho v^2}{g} \sin\theta\ d\theta \tag{3.6}$$

where v is the average linear velocity of the belt. As shown in Figure 3.4 symmetry causes the y-components of distributed centrifugal force at θ and $(\pi - \theta)$ to cancel each other. $\frac{\rho v^2}{g}$ may be considered constant in normal belt drive situations, and the x-component of centrifugal force may be integrated over $[0, \pi]$ to yield the tangential centrifugal force addition to the free span load. A force summation on Figure 3.4 in the horizontal direction yields:

$$2T_c = \frac{\rho v^2}{g} \int_0^{\pi} \sin \theta \, d\theta \tag{3.7}$$

$$2T_c = 2 \frac{\rho v^2}{g} \tag{3.8}$$

$$T_c = \frac{\rho v^2}{g} \tag{3.9}$$

Because of the symmetry of the pulley, the added centrifugal tension is divided equally between the tight and slack spans. Hence:

$$F_1 = T_1 + \frac{\rho v^2}{g} \tag{3.10}$$

$$F_2 = T_2 + \frac{\rho v^2}{g} \tag{3.11}$$

where F_1 and F_2 are the total free span tensions of an operating torque loaded drive. The expressions for F_1 and F_2 replace T_1 and T_2 in Equation 3.1 for a belt drive in motion, but the centrifugal effects cancel upon substitution. F_1 and F_2 replace T_1 and T_2 in Equation 3.2, but the distributed centrifugal force on the back side of the pulley necessitates the addition of another term, $2a \frac{\rho v^2}{g}$, to the right hand side of this equation and it reduces to its previous form also. Hence, Equations 3.1 and 3.2 are still valid. The forces, F_1 and

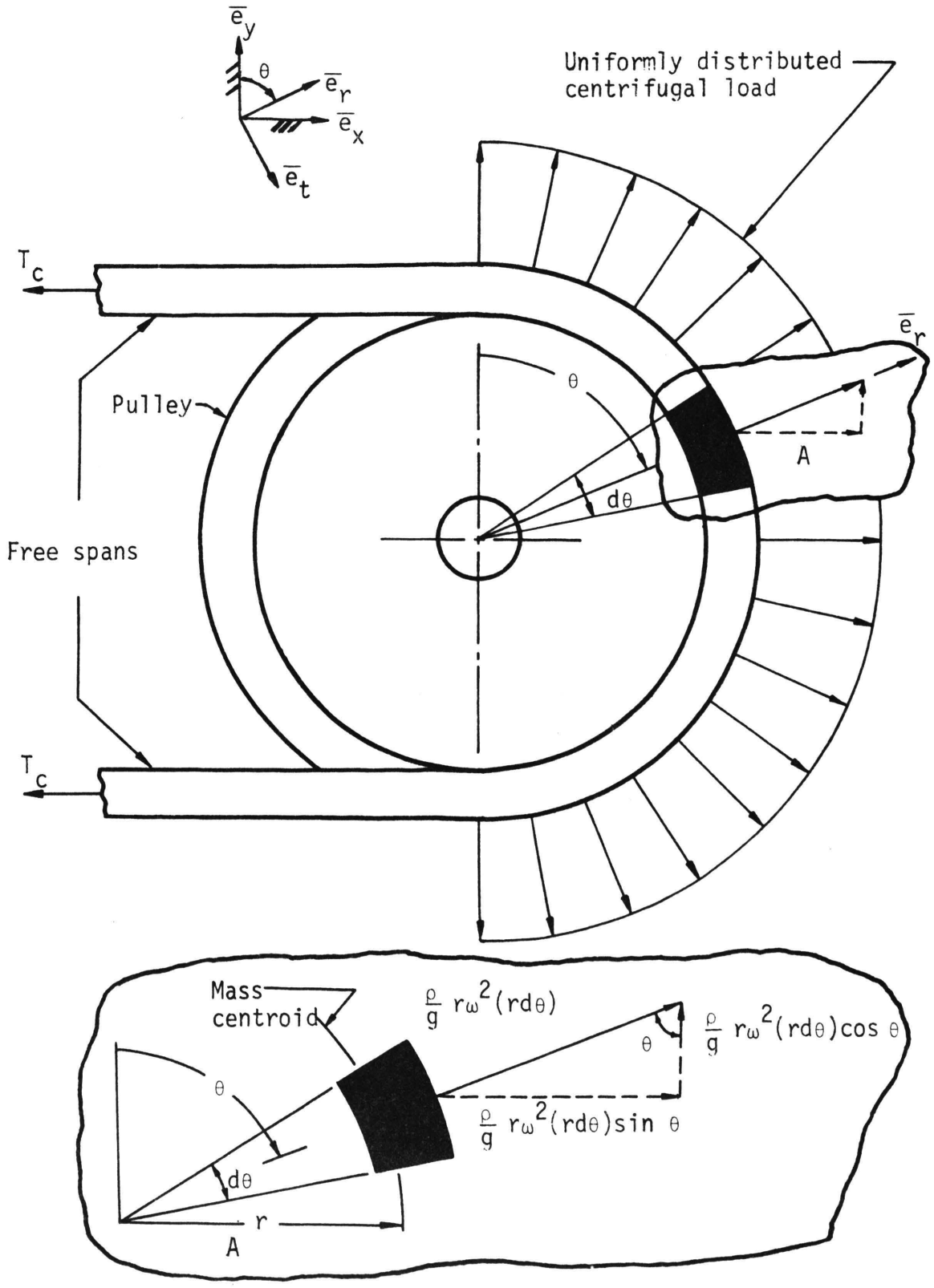

Figure 3.4. Consideration of Centrifugal Force Effects on a V-belt Drive

F_2, are the total free span tensions of the moving torque loaded drive. These forces may be used to determine the stress distribution in a plane of belt normal to the direction of motion given the construction of the belt and the geometry of the drive system.

Analytical models of cross sectional stress distributions in v-belts are given in literature referenced in Section II. Because of the difficulty of instrumenting several elevations at several axial positions in the cord and rubber matrix of a v-belt, experimental verification of these models has not been carried out. In this investigation, however, an attempt was made to analyze one of the most significant elevations in the belt cross section, namely the top of the cord layer. As described in Section IV, an analysis of load stress variation by photographic and electronic methods was attempted on a set of belts specially fabricated for this study without top covers in order to expose the cord layer.

Because the cord layer is generally relatively thin and ribbon-like, most analyses consider load stress distributed uniformly in the radial direction through the cord layer. Since cord stress varies almost linearly with cord strain, belt cord moduli furnished by the Dayco Corporation was used in the present study to convert strain data into stresses.

In order to determine the stress distribution in v-belt cords strictly due to bending around pulleys, the maximum bending stress term advanced by Marco, Starkey, and Hornung [10] was derived from a generalized bending analysis. Because the thickness of the cord layer was less than two percent of the pulley radius, the large

radius bending strain analysis shown in Figure 3.5 was considered valid. The assumptions are that a neutral axis of zero bending strain exists at some radius r from the pulley center and that plane transverse cord cross sections remain radially orientated during bending as shown in Figure 3.5. If e is the radial eccentricity of a fiber with respect to the neutral axis and if e is considered positive in the radially outward direction, then the bending strain in a fiber e units from the neutral axis as shown in Figure 3.5 is

$$\varepsilon_B = \frac{(r + e)(\Delta\theta) - r(\Delta\theta)}{r(\Delta\theta)} \tag{3.12}$$

$$\varepsilon_B = \frac{e}{r} \tag{3.13}$$

Positive values of ε_B denote tensile bending strains and negative values of ε_B denote compressive bending strains. Bending strains can be converted into bending stresses by the use of the tensile cord modulus, E_t, for tensile bending strains and the compressive cord modulus, E_c, for compressive bending strains.

$$\sigma_{B_t} = E_t \frac{e}{r} \tag{3.14}$$

$$\sigma_{B_c} = E_c \frac{e}{r} \tag{3.15}$$

If the belt is statically preloaded by a force producing a strain level ε_p and stress level σ_p in the free span, one finds the total strain on top of the cord layer at a point in the wrap to be

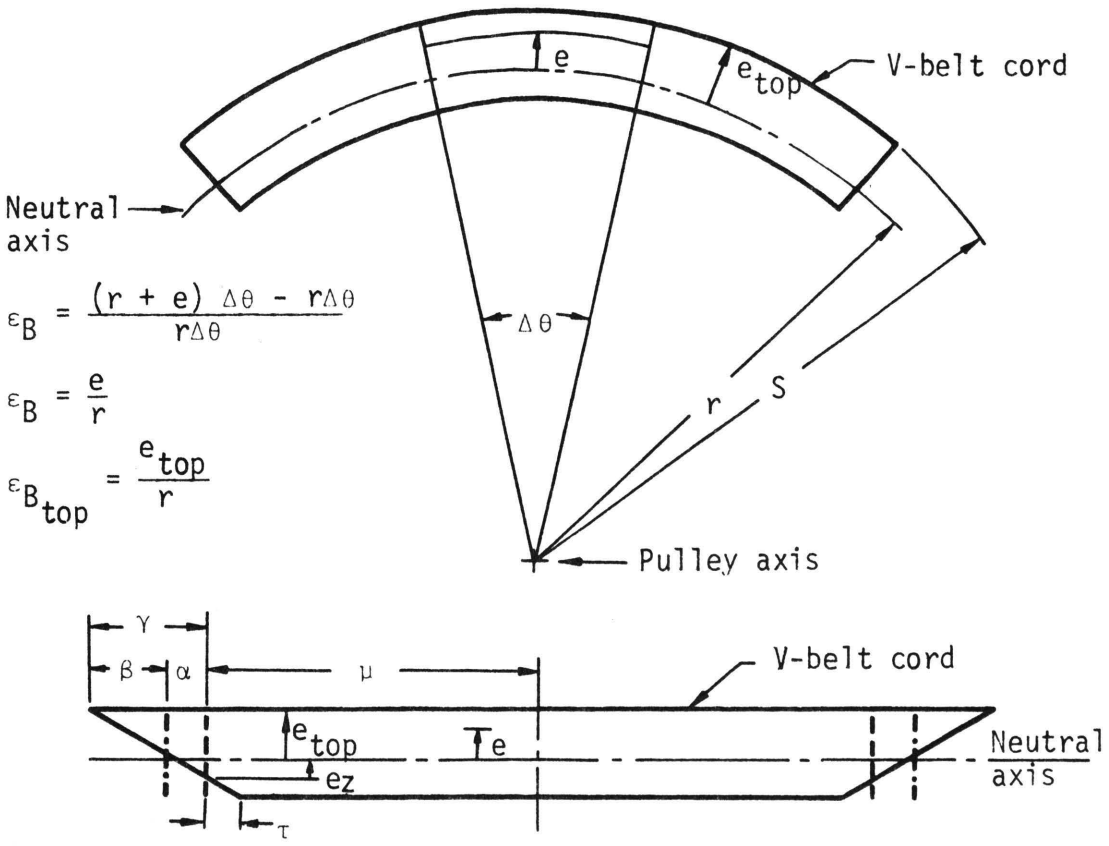

$$\varepsilon_p = \frac{\alpha}{\mu}\ *$$

$$\varepsilon_{tot} = \frac{\alpha + \beta}{\mu}\ *$$

$$\varepsilon_{B_{top}} = \frac{\beta}{\mu}\ *$$

$$\varepsilon_u = \frac{\tau}{\mu}\ *$$

Figure 3.5. Geometry of Large Radius Bending Strain in V-belt Cords

* α, β, γ, τ and μ are dummy values for lengths used in this figure only.

$$\varepsilon_{tot} = \varepsilon_P + \frac{e_{top}}{r} \tag{3.16}$$

and the stress

$$\sigma_{tot} = E_t \, \varepsilon_{tot} \tag{3.17}$$

The expression for bending strain on top of the cord layer is

$$\varepsilon_{B_{top}} = \varepsilon_{tot} - \varepsilon_P = \frac{e_{top}}{r} \quad . \tag{3.18}$$

For e_{top} equal to the elevation of the top of the cords with respect to the neutral axis and S equal to the radius of the cord top with respect to the center of the pulley, Equation 3.18 becomes

$$\varepsilon_{tot} - \varepsilon_P = \frac{e_{top}}{S - e_{top}} \quad . \tag{3.19}$$

Now if ε_{tot} and ε_P are experimentally determinable from the uncovered belts used in this experiment and S is measurable, then e_{top}, the eccentricity of the top of the cord layer with respect to the neutral axis, may be calculated.

$$e_{top} = \frac{S \, (\varepsilon_{tot} - \varepsilon_P)}{1 + (\varepsilon_{tot} - \varepsilon_P)} \tag{3.20}$$

Linear strain variation in the cords allows calculation of e_z, the elevation of zero stress from the geometry of Figure 3.5.

$$e_z = -e_{top} \frac{\varepsilon_P}{\varepsilon_{B_{top}}} \tag{3.21}$$

Also the strain in the bottom of the cord layer, ε_u, may be expressed as

$$\varepsilon_u = \varepsilon_{tot} - \left(\frac{D}{e_{top}} \varepsilon_{B_{top}}\right) \tag{3.22}$$

where D is the diameter of a cord. Application of Equations 3.13 through 3.22 to the experimental situation may be found in Section IV.

The simplest complete analysis of v-belt stress considers the cord layer to carry approximately 96% of the total belt load stress and 96% of the centrifugal stress distributed uniformly among the cords. Bending strain over the pulleys is considered as varying with radial eccentricity, e, as described by Equation 3.13 and also in some manner across the cord layer in the axial direction. The generalized cord stress equation for a given wrap position, θ, a given eccentricity, e, is

$$\sigma_{cord} = .96\left[\frac{T(\theta)}{A\ n} + \frac{\rho v^2}{g\ n\ A}\right] + E_{t,c}\frac{e}{r} \tag{3.23}$$

where E_t is used for radial positions outward from the elevation of zero stress and E_c is used for eccentricities radially inward from the elevation of zero stress. In Equation 3.23, A is the cross sectional area of a cord, and n is the number of cords in the cord layer. $T(\theta)$, the load tension, must be determined by an experimental stress analysis or by an analytical analysis such as that of Hornung [7] or Martynov [11] which incorporate belt parameters and drive geometry

into the calculation of load tension or stress with respect to wrap angle, θ. The eccentricity term in Equation 3.23 must be evaluated by an experimental determination of neutral axis location such as that described in Section V because there is presently no theory which describes the change in neutral axis position with respect to pre-load and pulley size. The linear velocity of a belt drive used in the centrifugal stress term of Equation 3.23 may be determined to sufficient accuracy by averaging the speed of the tight and slack belt spans as determined by a hand tachometer with a linear velocity attachment. Equation 3.23, then, is a simplified but complete total stress equation for v-belt cords and is suitable for evaluation using experimentally determinable quantities.

Accompanying cyclic stress variation due to torque transmission in v-belt drives is the phenomenon of belt motion relative to the pulleys. Total belt motion may be considered as consisting of absolute pulley motion plus radial and tangential motion of the belt with respect to the pulley. Analyses of the relationship between belt stress and other drive parameters with respect to belt motion have been performed analytically and are reported in the literature [4, 11, 12, 16]. Regardless of local effects, the gross effect of all belt creep and slip is the total percent of input power lost between the driver and the driven pulleys. This fractional power loss term may be written as

$$s_{tot} = \frac{FR_R N_R - FR_N N_N}{FR_R N_R} \tag{3.24}$$

where FR_R and FR_N are torques on the driver shaft and driven shaft, respectively, and N_R and N_N are the speeds of the driver and driven shafts, respectively. If frictional torque losses are small, then FR_N approaches FR_R and

$$s_{tot} = \frac{N_R - N_N}{N_R} \quad . \tag{3.25}$$

s_{tot} has been considered by Martynov [11] and others to be composed of four main components:

$$s_E = \frac{T_1 - T_2}{M_t} = \frac{v_1 - v_2}{v_1} \text{ (elastic creep)} \tag{3.26}$$

$$s_R = \frac{\omega_R r_R - v_1}{w_R r_R} \quad \text{(driver run-on slip)} \tag{3.27}$$

$$s_N = \frac{v_2 - \omega_N r_N}{v_2} \quad \text{(driven run-on slip)} \tag{3.28}$$

$$s_T = 1 - \frac{r_N/r_R}{r_N'/r_R'} \quad \text{(transmission ratio slip)} \tag{3.29}$$

(Primed quantities are calculated for a dynamic torque loaded drive.)

where

$$s_{tot} = s_E + s_R + s_N + s_T \tag{3.30}$$

and the symbols in Equations 3.26 through 3.29 are defined on page vii. Elastic creep was previously defined as the change in tangential elastic deformation of the belt due to the change in tension between

T_1 and T_2 as the belt passes around the driver or driven pulley. Driver run-on slip results from the fact that the linear velocity of the tight span is slightly less than the linear velocity of the pitch radius of the driver pulley. Driven pulley run-on slip is the resultant of the fact the slack span linear velocity is slightly more than the linear velocity of the pitch radius of the driven pulley. Transmission ratio loss results from the difference in the pitch radius of the belt on driver and driven pulleys while in the process of high speed torque transmission.

An important drive parameter associated with the calculation of belt power losses is the traction coefficient, ψ. The definition of ψ is simply

$$\psi = \frac{T_1 - T_2}{T_1 + T_2} \tag{3.31}$$

Belt power loss, s_{tot}, has been found to vary linearly with the traction coefficient over the acceptable design range of torques and preloads for a given belt drive situation. Above a certain traction coefficient, ψ_o, slip losses increase at an increasing rate yielding instability of the drive and gross heat generation. A graph of percent power loss versus traction coefficient determines linear steady state range of torque and preload for a belt drive. An analysis of several drive situations by this method is included in this study.

IV. BASIC TEST EQUIPMENT

The test apparatus was designed as a two pulley drive for the simulation of common automotive torque loads, preloads, pulley diameters, and speeds. The pivoted drive setup as shown in Figures 4.1 and 4.2 was chosen to facilitate the quick calculation of free span tensions. The known free span tensions then served as a reference for calibration of the equipment used to measure stresses around the pulleys.

The driver pulley was powered by a cradled variable speed D.C. motor (a)*. A stator mounted torque arm on the motor operated a balance scale (b) for torque determination as shown in Figure 4.1. The driver pulley was set clear of the motor so that instrumentation could be placed on either side of it.

Two automotive alternators (c) were vertically aligned on the pivot platform and connected by a belt as shown in Figure 4.4. The alternators were provided with field voltage from a variable voltage D.C. supply (d). The shaft of the lower alternator was connected through a flexible coupling to a bearing mounted extension shaft which held the driven test pulley. The extension shaft displaced the driven test pulley from the face of the alternator to provide space for instrumentation around it. When uncoupled from the alternators, the extension shaft provided a nearly friction free drive for testing belts in the unloaded condition. Power output from the alternators

*Lower case letters refer to equipment descriptions given in Appendix A.

1. Balance scale
2. Torque arm
3. Cradle bearing housing
4. Variable speed D.C. motor
5. Test belt
6. Alternators
7. Hinged yoke
8. Force transducer
9. Suspended pulley
10. Preload weight platform
11. Force transducer indicator
12. Output of alternators (to resistor bank)
13. Variable voltage field supply
14. Driver test pulley
15. Driven test pulley
16. Pivoted platform

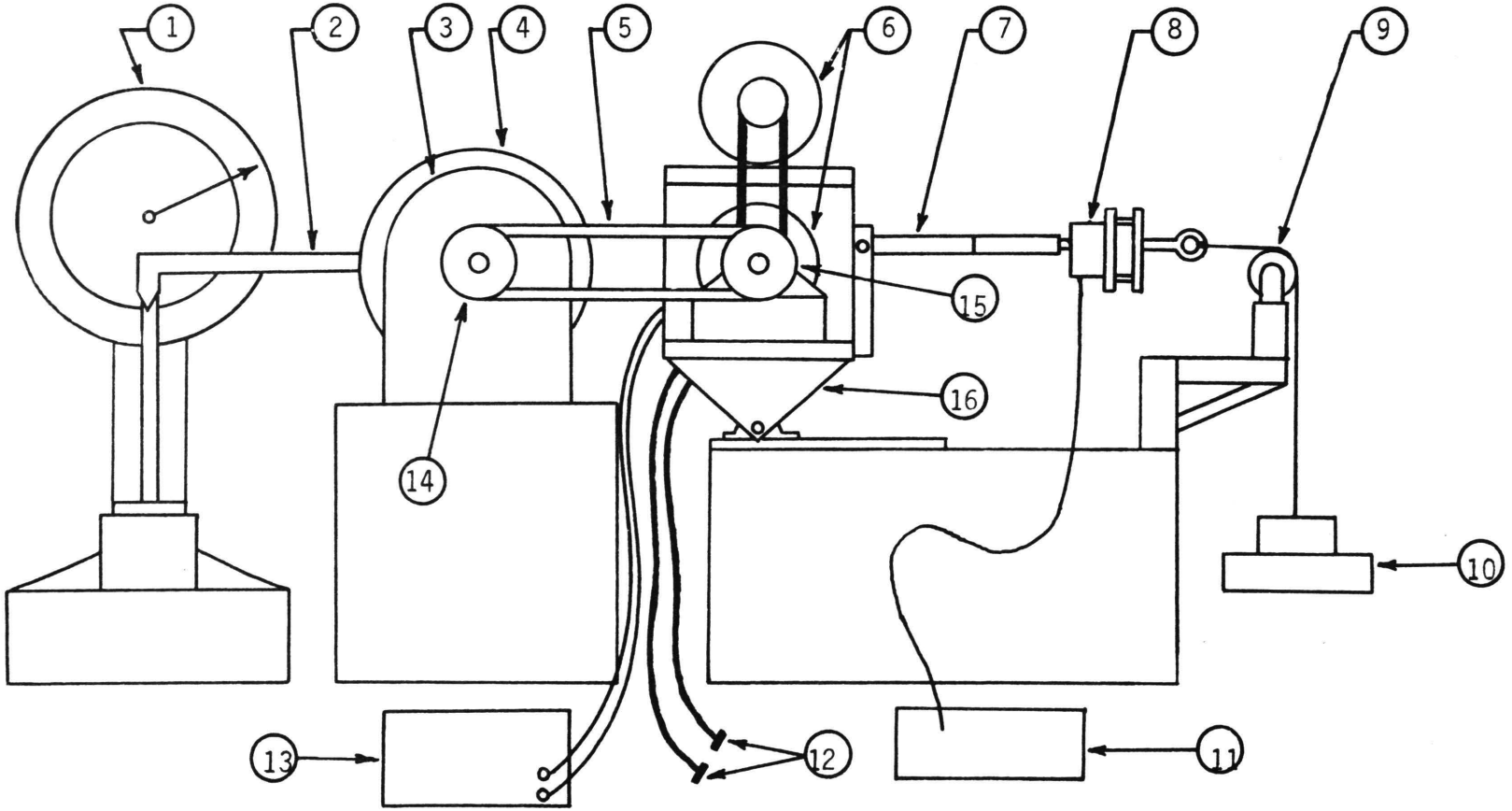

Figure 4.1. Schematic of Basic Test Equipment

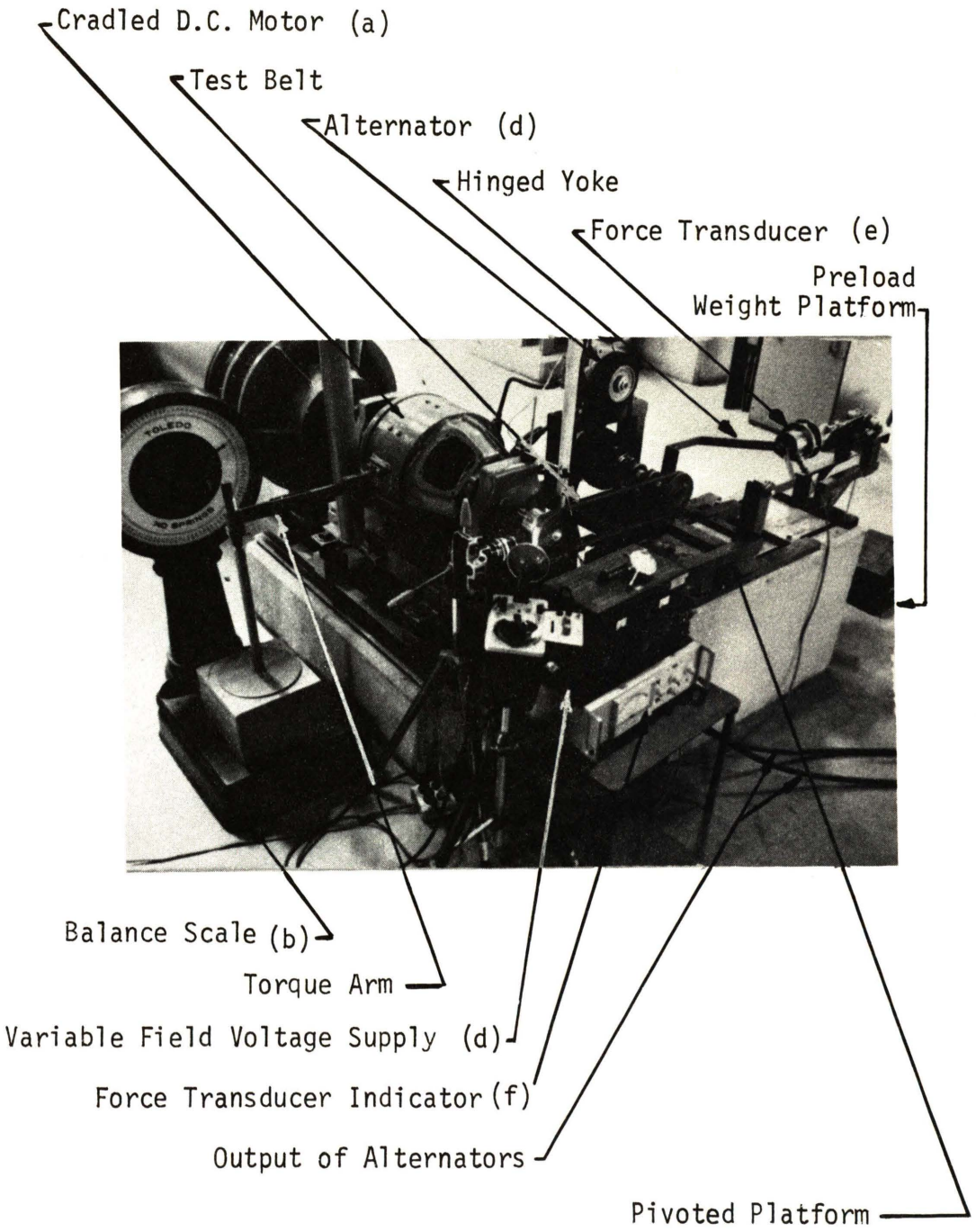

Figure 4.2. Photograph of Basic Test Apparatus

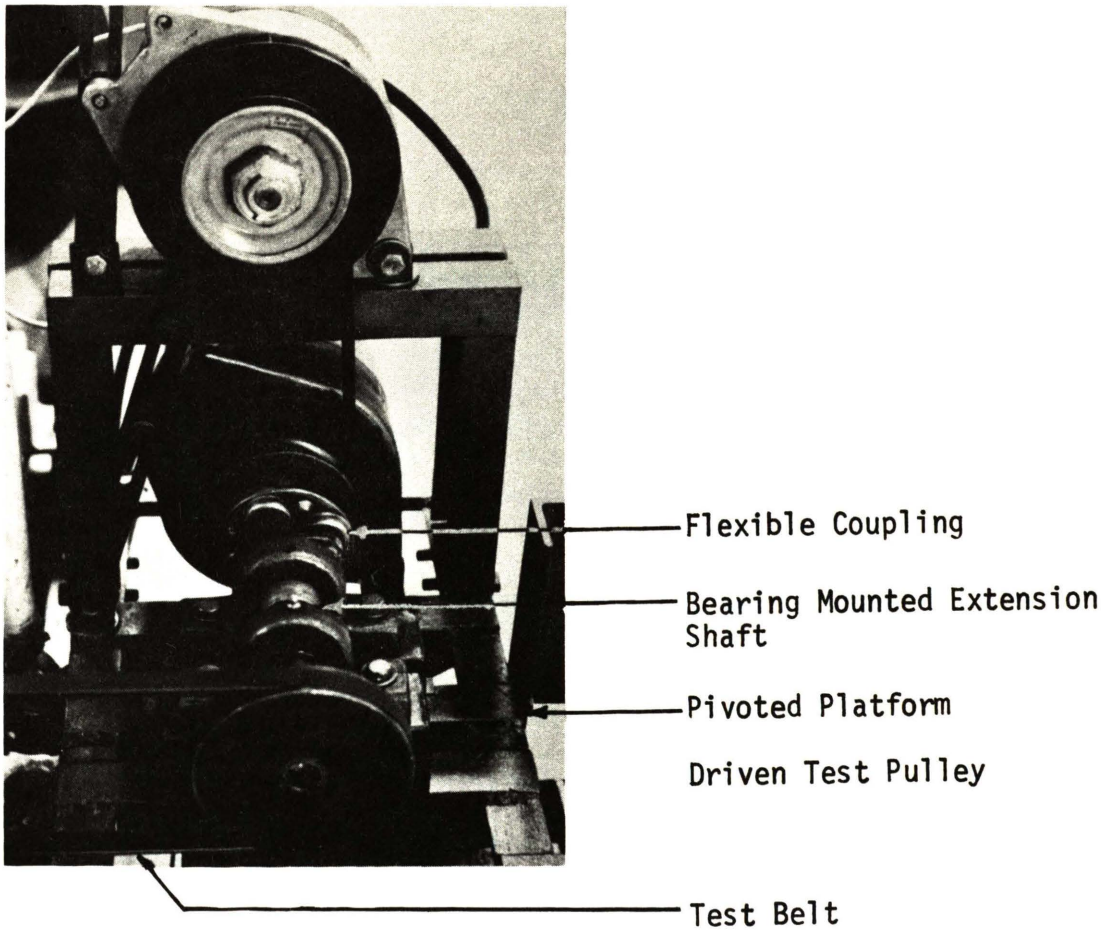

Figure 4.3. Closeup of Driven Pulley Linkage

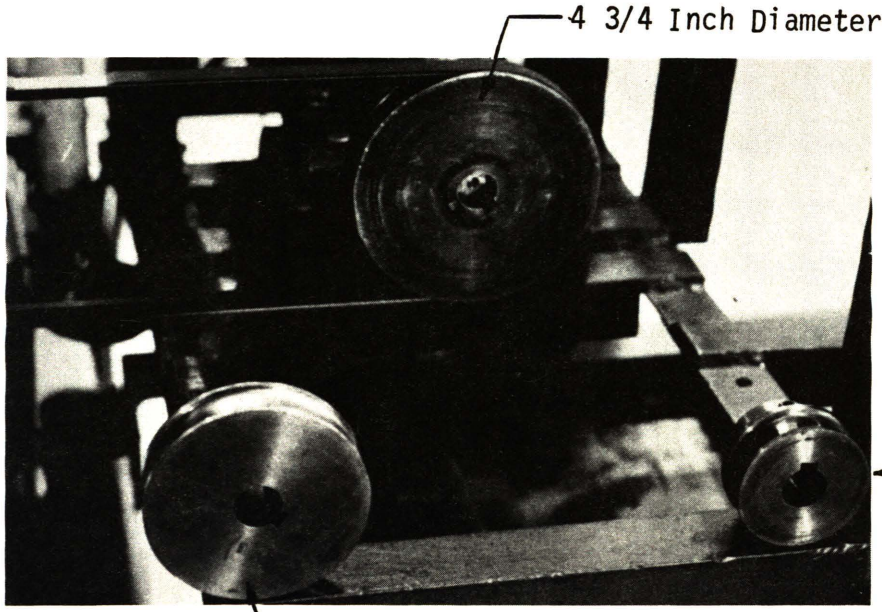

Figure 4.4. Machined V-Pulleys used in Experimentation

was absorbed in a large resistor bank.

The advantages of this particular absorbtion system were as follows. First, alternators represent one of the components driven by automotive v-belts and the power they produce may be led away from the pivot platform by flexible cables which do not exert extraneous moments about the pivot axis. Second, the variable field voltage supply provided for variation of the torque load from zero to the combined load of the two alternators simply by changing the field voltage.

The constant tensioning device consisted of a hinged yoke leading from the back of the pivot as shown in Figures 4.1 and 4.2. An electronic force transducer (e) was connected to the center of the yoke and a cable led from the back of the transducer over a suspended pulley to the weight platform. The force transducer was wired to a Daytronic Transducer Indicator (f). This arrangement allowed for accurate determination of the belt pretension load.

The basic system provided variables in the automotive range. Torqes from 2 to 10 pound feet were obtainable at speeds from 200 to 3600 RPM. Values for the total preload, the sum of the two span tensions, could be varied from 0 to 300 pounds.

The test pulleys (Figure 4.4) used in this experiment were supplied by the Dayco Corporation and were made of high quality machined steel in order to provide the truest possible sheave width for smooth operation of the belt system. Pulleys with 2 1/4, 3 1/2, and 4 3/4 inch diameters were used for all the tests. Comparisons of results for equal increments in pulley diameter were possible from

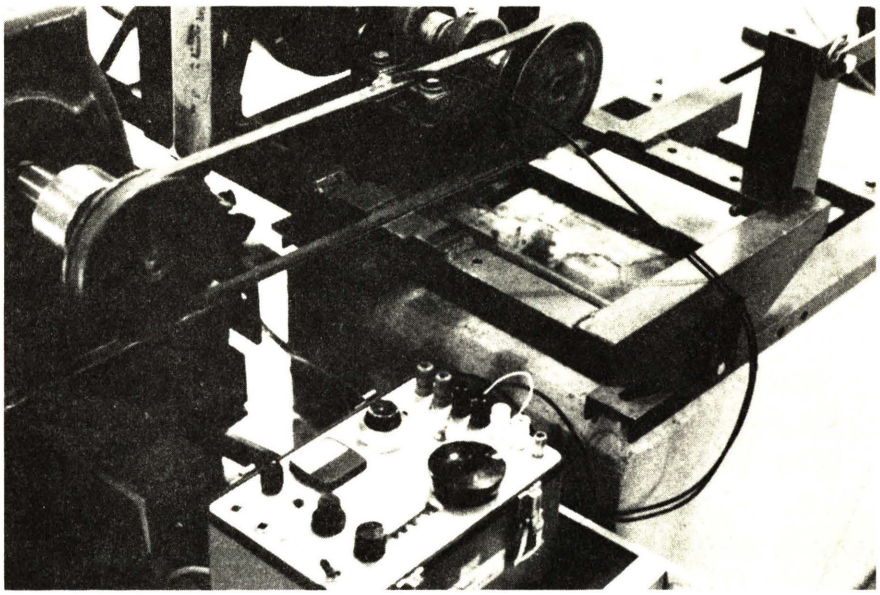

Figure 5.1. Overall View of Strain Gaged Belt System

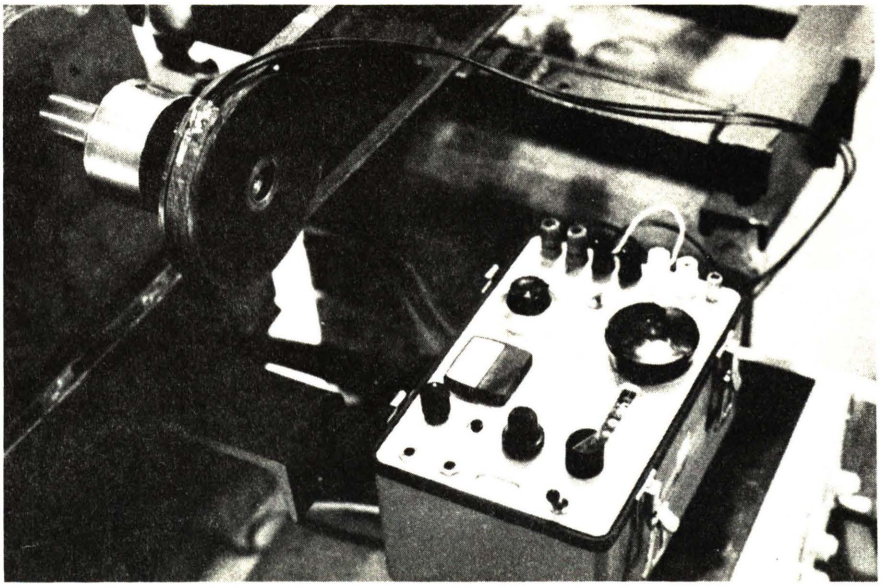

Figure 5.2. Closeup of Strain Gage Rotated to a Position in the Wrap Angle

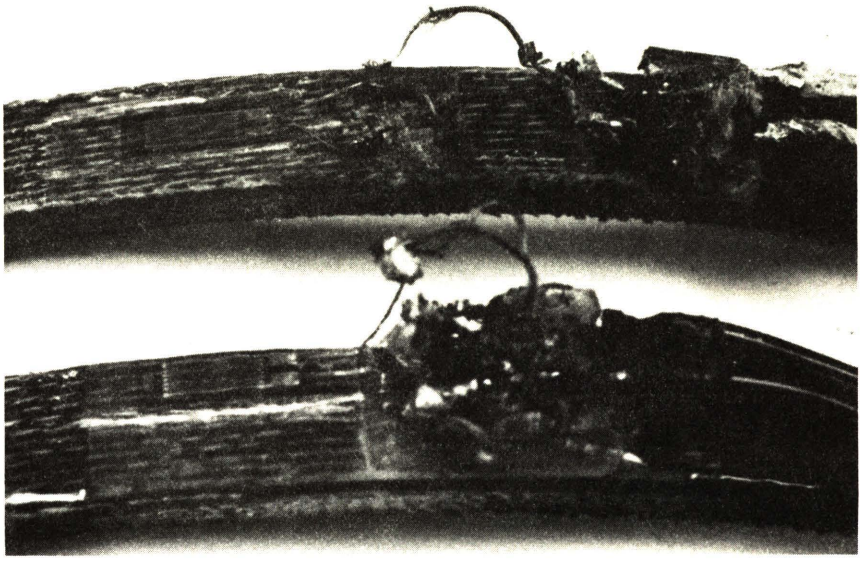

Figure 5.3. Center and Edge Mounted Strain Gages on High Modulus Exposed Cord Belt (g)

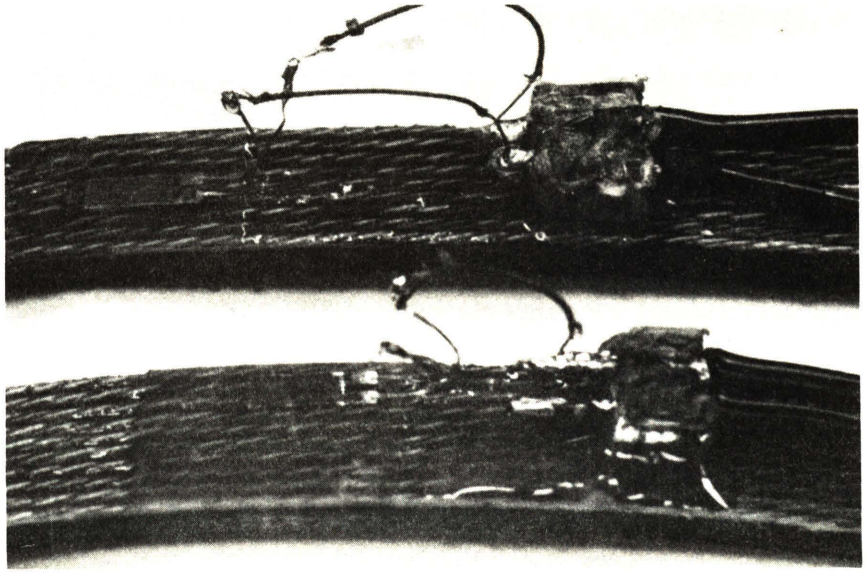

Figure 5.4. Center and Edge Mounted Strain Gages on Low Modulus Exposed Cord Belt (h)

in Figures 5.3 and 5.4. The two lead wires were taken to the strain indicator (m) and a quarter bridge circuit was completed. The gage factor was set to 2.095 and the indicator was adjusted to balance the bridge. Strain readings from the midpoint of the free span were considered to be the result of the uniformly distributed free span tension. Several strain readings were averaged near this point to obtain the strain level corresponding to the span tension. The instrumented belt was then slowly rotated from the midpoint of the free span to the center of the wrap angle as shown in Figure 5.2 with strain readings recorded every inch in the span and every 15 degrees in the wrap. The gage was translated back to the free span and readings were again taken. The two sets of strain data were averaged to nullify any effects, if present, due to the direction of rotation. The displacement of the belt during this test covered a symmetric quarter cycle of belt travel so that the strain profiles of the other three quarters would be equivalent to that of the tested quarter. Center and edge gage tests were run for belt types (g) and (h) for the 2 1/4, 3 1/2, and 4 3/4 inch diameter pulleys at three preloads yielding $(T_1 + T_2)$ between 50 and 270 pounds for a 36 run matrix. Maximum strain change between free span and wrap center ranged from approximately 10,000 to 30,000 microstrain. The incomplete runs on the 2 1/4 inch diameter pulleys were due to the fracture of the 5 percent gages at high preloads. The average fully developed strain in the wrap minus the mid-free span reading was set equal to the bending strain, $\frac{e_{top}}{r}$. Since both e_{top} and r were unknown, r was replaced by $(S - e_{top})$ where S was the measured radius

of the top of the cord layer with respect to the pulley axis. The equation for determining e_{top} was then

$$\varepsilon_{B_{top}} = \varepsilon_{tot} - \varepsilon_P = \frac{e_{top}}{S - e_{top}} \tag{5.1}$$

Solving for e_{top}, Equation 5.1 yields:

$$e_{top} = \frac{(\varepsilon_{tot} - \varepsilon_P)\ S}{1 + (\varepsilon_{tot} - \varepsilon_P)} \tag{5.2}$$

The experimental bending stress was determined from the bending strain, the tangential cord modulus, M_{cord}, and the cross sectional area of a cord, A.

$$\sigma_B = \frac{M_{cord}}{A} \quad \varepsilon_B \tag{5.3}$$

The total stress on the top of the cord layer for a point in the pulley wrap is then

$$\sigma_{tot} = \sigma_P + \sigma_{B_{top}} \tag{5.4}$$

where σ_P is defined as 96 percent of the free span tension distributed uniformly across the cord layer.

$$\sigma_P = \frac{.96\ T}{n\ A} \tag{5.5}$$

The analysis was completed with the calculation of the elevation of zero stress and the strain in the bottom fibers of the cord as shown in Equations 3.21 and 3.22.

B. DYNAMIC STRESS ANALYSIS

After acceptable results were obtained from static strain gage tests, experimentation was continued with attempts to measure the variation in load stress due to torque transmission over the driver and driven pulleys. Again, the three pulley sizes employed were 2 1/4, 3 1/2, and 4 3/4 inches in diameter. The system was designed to deliver a maximum of 10 pound feet of torque from which the maximum tension differences can be calculated by Equation 5.6.

$$T_1 - T_2 = \frac{FR_R}{r_R} \tag{5.6}$$

For FR_R equal to 120 pound inches and r_R equal to 1.125, 1.175, and 2.375, the three pulley radii, the maximum tension differences obtainable were approximately 106 pounds, 69 pounds, and 51 pounds on the 2 1/4, 3 1/2, and 4 3/4 inch diameter pulleys, respectively. Considering 96 percent of the tensile load to be evenly distributed among the belt cords, the maximum cord strain change was calculated from Equation 5.7.

$$\Delta\varepsilon_{\substack{max \\ load}} = \frac{.96\ (T_1 - T_2)}{M_{cord}\ n} \tag{5.7}$$

The maximum cord strain change between tight and slack sides of the low modulus belt was calculated as 0.0061, 0.0040, and 0.0029 inches per inch, and for the high modulus belt 0.0020, 0.0013, and .00096 inches per inch for the three pulley sizes used in this study.

1. PHOTOGRAPHIC STRESS MEASUREMENT

With the maximum range of load strain established, a time synchronized photography system was developed in order to measure

the increments in load strain as the belt passed around the pulley. The problem of camera shutter synchronization with a small marked spot on a moving belt was addressed first. A Miranda 35 millimeter camera (n) was fitted with three extension tubes totaling 2 1/4 inches and was focused on the belt. Exposure time was set to exceed the time of one complete belt cycle. The x-contacts of the camera were wired to the external control jack of a General Radio flash delay unit (o). The input trigger terminal of the flash delay was connected to a photoelectric pickoff (p) focused on the underside of the belt as shown in Figures 5.5 and 5.6. The strobotac input plug was connected to a General Radio Strobotac (q) which was focused on the same spot as the camera. A 1/8 inch by 1/4 inch piece of aluminum foil was cemented to the underside of the belt as a target for the photoelectric pickoff. The flash delay was set to the multiple pulse mode and the strobe was set to external trigger. Then the strobe, flash delay, and belt drive were turned on. The strobe pulsed each time the foil strip passed under the photoelectric pickoff. The range of the flash delay was adjusted so that the strobe pulsed on the marked belt section as it appeared in front of the camera lens. The flash delay was switched to the single pulse mode and the camera shutter was tripped. While the camera shutter was open, a single high intensity strobe pulse 3.0 microseconds in duration flashed on the belt while the marked section was in front of the camera. The extremely short duration of the flash caused an apparently still image of the belt on the film. For this work, Kodak Tri-X film was used with the camera f-stop set to 16 to provide maximum field depth.

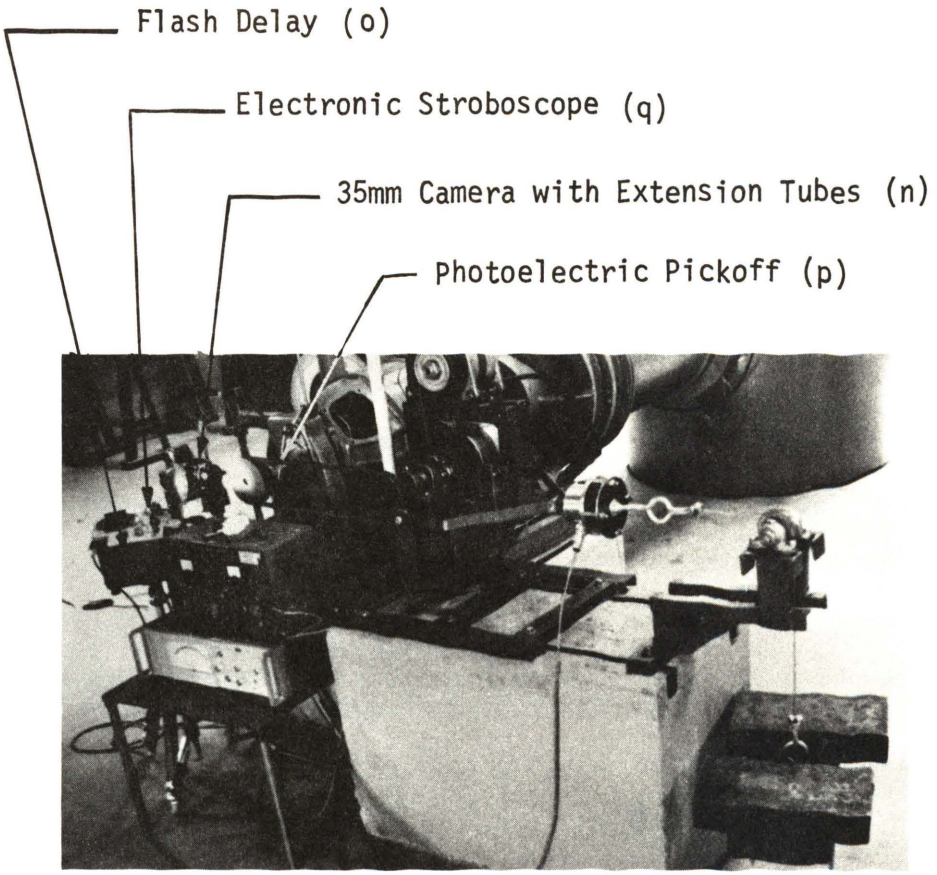

Figure 5.5. High Speed Photographic Synchronization System

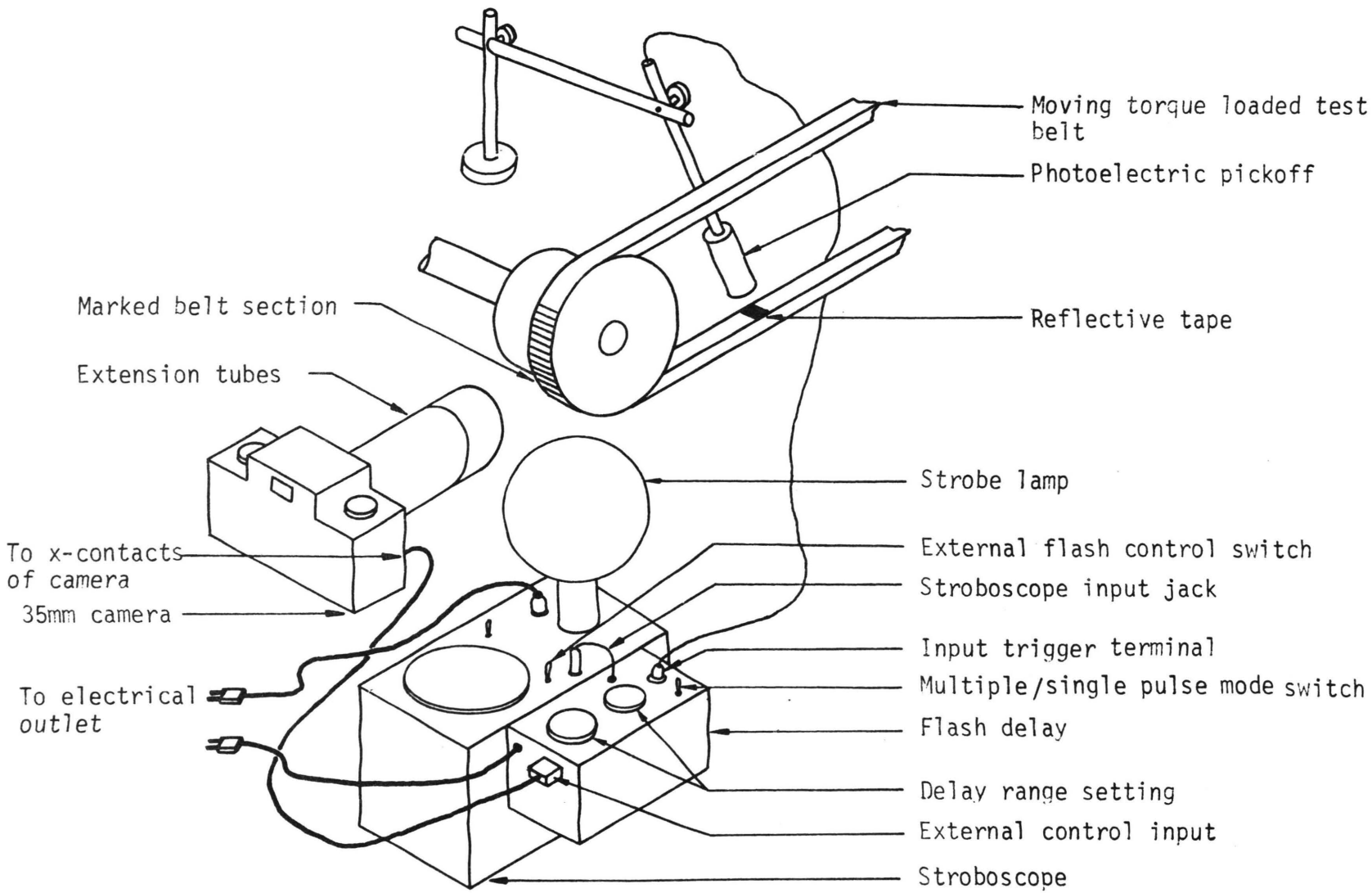

Figure 5.6. Schematic of Photographic Synchronization System

Examples of the camera synchronization with the designated belt section using the equipment described are shown in Figure 6.12.

In addition to the high speed synchronization of the photographic system, the calibration of measurements from photographs was also necessary. Photographs of a static free span of belt were taken on the setup shown in Figure 5.5 at preloads yielding span tensions between 5 and 166 pounds per span. The camera was not moved and the focus was not readjusted during the entire shooting sequence in order to preserve the size of the photographed image. The photographed belt segment was first covered with white India ink and then lines were scribed on it by drawing a knife edge across the top surface of the belt. The width of the lines was less than 1/100 inch as shown in Figure 6.13. The photographic film was processed in Kodak D-76 developer. Developed negatives were placed in a photographic enlarger and magnifications of approximately 20 times were accomplished on the enlarger table. Measurements from the image projected on the enlarger table were attempted with a machinist's scale but repeatable strain measurements could not be made. The high enlargement of the photographic negative widened the marker lines as well as the distances measured, hence increasing the error in a given measurement.

In order to increase resolution, a photographic negative was placed on the table of an overhead projector (v) and the image was projected to a smooth white vertical surface with an enlargement of about 30 times. A cathometer microscope (r) capable of measuring distances as large as 25 millimeters with accuracy of 0.01 millimeter

was set about eight feet from the image and focused on it. Repeatable measurements could not be made by this method, however, because of the uncertainty of the scribed edge due to the film grain size and lack of contrast at high enlargements. Development of film on photographic paper for the purpose of making measurements was considered unacceptable for this work due to the high enlargement factor necessary and the inherent shrink and stretch of photographic paper as it dries. Further analysis of the photographic method is included in Sections VI and VII of this report.

2. MAGNETIC PICKOFF-COUNTER STRESS MEASUREMENT

Another attempt at measuring load strains in a dynamic torque loaded belt drive was made with the magnetic pickoff (s) and 100 nanosecond counter (t) shown in Figures 5.6 and 5.8. The input leads of the pickoff were connected across 12 volts D.C. and the output leads were connected to the timer. When one of the staples in the belt shown in Figure 5.8 passed under the pickoff, a 5 volt D.C. pulse was sent from the pickoff to the timer to initiate a time count. Another pulse sent to the timer by the second staple terminated the count. The velocity of the belt was then calculated as the length between the two staples divided by the time of passage for the two closely spaced staples shown in Figure 5.8. Constant mass theory provided correlation between changes in stress and changes in velocity. The adjustable display time on the counter allowed for the continuous sampling of data. The pickoff was mounted off a bearing on the driven shaft to insure constant radial distance settings for differing angular positions.

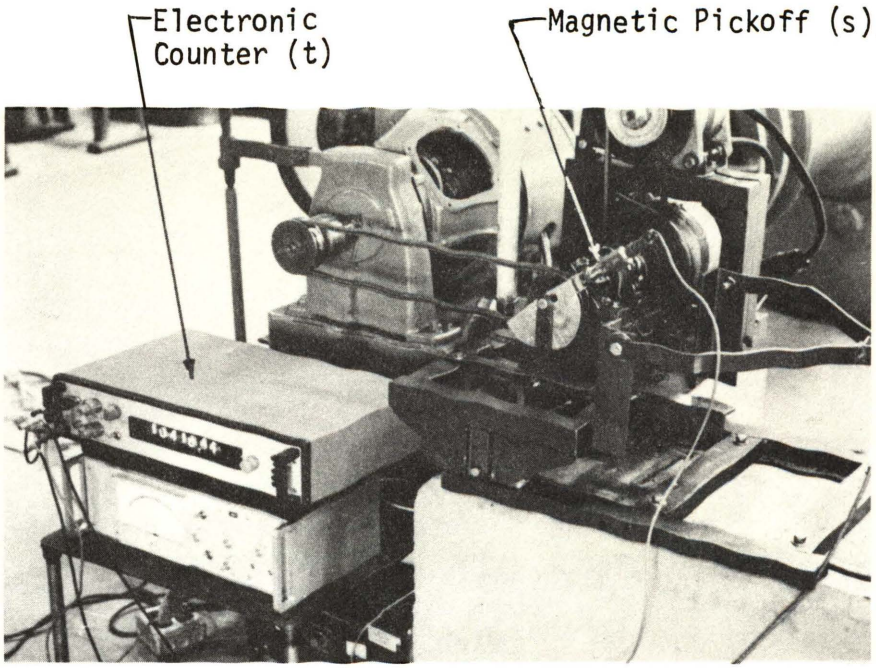

Figure 5.7. Magnetic Pickoff-Counter Instrumentation System

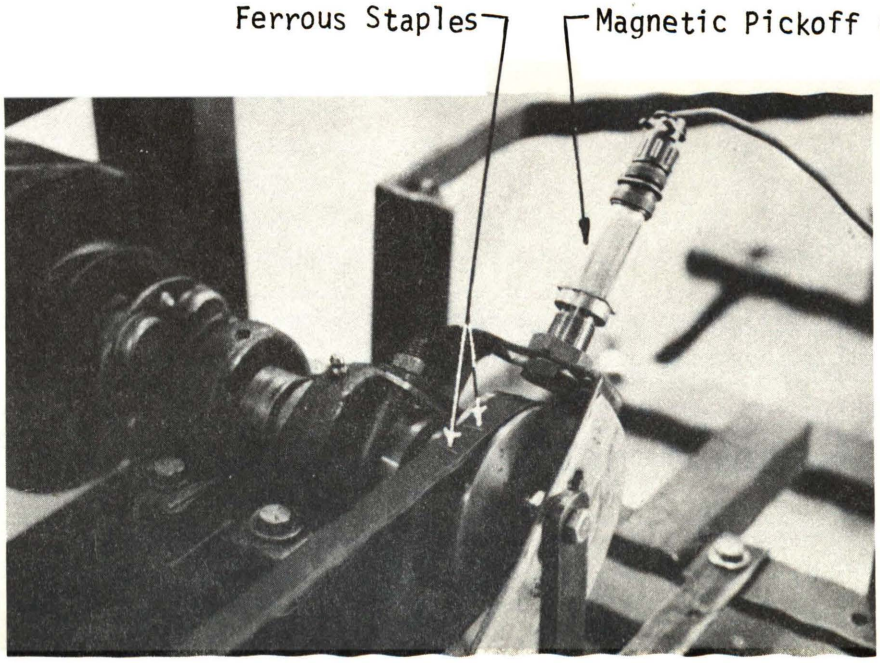

Figure 5.8. Closeup of Magnetic Pickoff and Target Staples

Timer readings obtained from positioning the magnetic pickoff at points around the pulleys produced a consistent set of readings, but appropriate increase in readings from the tight span to the slack span could not be established. Even the sudden increase in bending strain as the belt entered the wrap could not be discerned from timer readings in this region. The probable reason for this lack of correlation is discussed in Section VI of this report.

Subsequently, a large 1/4 by 3/8 inch staple was used as a trigger target for the magnetic pickoff. The timer was set to the duration mode so that it would begin counting on a positive voltage/time slope and cease counting on a negative voltage/time slope. The pickoff produced 5 volts D.C. when in the presence of the ferrous staple and zero volts D.C. at all other times. Hence, the timer registered the passage time of the 1/4 inch length when the belt drive was running. It was felt that this test would provide a better guarantee of a fixed length transducing section for calculation of belt stress using constant mass rate equations. Continuous data sampling was employed to obtain a set of readings which could be averaged at each point where data was taken. The readings obtained from the timer again showed no definite trends in velocity change around the pulley even when twenty to thirty readings were taken at each point and averaged. The stiffening of a section of belt with such a large staple was identified as a questionable practice because the change in belt properties in the stapled section might cause slip rate to vary and cause disruption of the continuous creep rate of the belt around a torque loaded pulley.

3. ANALYTICAL LOAD STRESS DETERMINATION

The effort to actually measure varying load strains on a moving torque loaded belt drive was suspended at this time. In order to complete the stress analysis, the Hornung [7] analytical belt tension equations were employed. A digital simulation program of the Hornung equations as described in Section II was run for the 2 1/4, 3 1/2, and 4 3/4 inch diameter pulleys. Torque loads between five and ten pound feet were simulated with total preloads, $T_1 + T_2$, ranging from 125 to 225 pounds for the high modulus belt. The matrix of simulation runs constituted the same tests which would have been accomplished experimentally if the testing techniques had been successful. The output of the Hornung simulation program was plotted in a series of tension versus wrap angle plots shown Figures 6.14, 6.15 and 6.16.

C. ANALYSIS OF TRANSMISSION POWER LOSSES IN BELT DRIVES

As a final dynamic test, total belt slip rate was measured for approximately the same set of drive situations for which the simulations were made in order to examine the design acceptability of these drives. Because the system was not originally designed for this test, no provision had been made to precisely measure torque on the output shaft. However, the simple tension analysis of Section III reveals that equality of torques on driver and driven pulleys is a relatively safe assumption. If input and output torques were equal, then the percent power loss between equal diameter driver and driven pulleys would be due solely to the percent differences in RPM between the pulleys. Hence, an attempt to measure the steady state losses in RPM was made by measuring the rotational speeds of driver and driven pulleys with

a hand tachometer (u) for several sets of drive conditions corresponding closely to those used in previous tests in this study. Appropriate data were taken for the determination of percent speed loss and traction coefficient for each run.

$$\% \text{ Speed Loss} = \frac{N_R - N_N}{N_R} \times 100\% \tag{5.8}$$

$$\text{Traction Coefficient} = \psi = \frac{T_1 - T_2}{T_1 + T_2} \tag{5.9}$$

The range of traction coefficients obtainable was limited to 0.90, 0.58, and 0.42 on the 2 1/4, 3 1/2, and 4 3/4 inch diameter pulleys, respectively, but the torque ranges between two and ten pound feet were most representative of automotive v-belt applications. The accuracy of the hand tachometer used for the RPM measurements was $\pm$ .25% and the RPM sampling process was repeated at least six times for each drive situation to minimize any start-stop errors caused by the tachometer. Tight and slack side tensions were computed for each run from Equations 3.3 and 3.4. Data gathering was terminated at the completion of this set of experimental runs.

VI. RESULTS

The purpose of this section is to present a quantitative analysis of v-belt stress and the stress-related power losses that are present in torque loaded belt drives. Bending and free span stresses were determined experimentally as described in Section V. Centrifugal belt tension was determined by the use of Equation 3.9. When attempts to experimentally measure the change in load stress due to torque transmission over the pulleys failed to produce meaningful results, the Hornung analytical belt tension analysis was used to complete the presentation of total v-belt stress in automotive drives. Belt power losses were examined in order to determine the acceptable design ranges of preload, torque load, and speed for the drive situations tested.

A. STATIC BENDING TEST RESULTS

The results of the static bending stress tests are shown in Figures 6.1 through 6.3. Figure 6.1 shows typical plots of stress versus displacement for a symmetric quarter cycle of belt travel. The points on this graph were determined in the following manner. First, several readings were taken from the strain gaged belts described in Section V within one inch of position A shown on Figure 6.1. These readings were averaged to produce a single reference strain reading which was assumed to correspond to the uniformly distributed free span cord stress, σ_p.

$$\sigma_p = \frac{0.96\ T}{n\ A} \tag{6.1}$$

The strain indicator was not zeroed at zero strain so that ε_{P_i}, the indicated preload strain, was not equal to ε_P.

$$\varepsilon_P = \frac{\sigma_P}{E_t} \tag{6.2}$$

E_t was defined as $\frac{M_{cord}}{A}$, the tangential tensile modulus of a single cord divided by the cross sectional area of a cord. The cord top stress at any other point in the belt cycle was called σ_{tot} and the indicated strain at that point, ε_{tot_i}. Hence,

$$\sigma_{tot} = \sigma_P + \frac{M_{cord}}{A} \left(\varepsilon_{tot_i} - \varepsilon_{P_i}\right) . \tag{6.3}$$

Next, a single average value of fully developed bending stress was determined from each stress-displacement profile. This was accomplished by averaging the values of $\left(\varepsilon_{tot_i} - \varepsilon_{P_i}\right)$ for strain readings taken between 30^o and 90^o in the wrap and by equating this average to the bending strain, ε_B, for a given pulley size and preload.

$$\varepsilon_{B_{top}} = \frac{\left(\varepsilon_{tot_i} - \varepsilon_{P_i}\right)_{30^o} + \left(\varepsilon_{tot_i} - \varepsilon_{P_i}\right)_{45^o} + \ldots + \left(\varepsilon_{tot_i} - \varepsilon_{P_i}\right)_{90^o}}{5} \tag{6.4}$$

The maximum tensile bending stress known to occur on top of the cord layer then became

$$\sigma_{B_{top}} = E_t \, \varepsilon_{B_{top}} \tag{6.5}$$

Figure 6.1 shows an actual set of stress profiles for a symmetric quarter cycle of a static untorqued drive. The center and edge gage readings were taken from strain gages mounted in the center and near the edge of the exposed-cord layer belts as described in Section V. A gage covered approximately three cords on the low modulus belt and four cords on the high modulus belt. The center and edge readings, then, were an average of the strain in the three or four cords which the gages covered. The strain gages were 1/4 inch long. This length represents 12.74, 8.19, and 6.03 degrees of arc on the 2 1/4, 3 1/2, and 4 3/4 inch diameter pulleys, respectively. Where abrupt bending strain changes occur, the strain readings represent an average strain value over the appropriate arc length.

As shown in Figure 6.1, both center and edge mounted gages produced nearly constant strain readings for several inches of travel near the center of the free span. As the gages approached the pulley, there was a redistribution of the static load with edge stresses increasing and center stresses decreasing. The redistribution became more severe for increasing preloads and was noted on both belt types and all three pulley sizes tested. Fully developed stress in the wraps differed significantly from the center to the edge of the belt (Figure 6.1). Graphs such as Figure 6.1 are not shown for all the test runs made because of their similarity in shape. Significant values from a single test run are the first value, σ_P, and the average of the last five values of $\left(\sigma_P + \sigma_{B_{top}}\right)$. To illustrate these values, Figures 6.2 and 6.3 were plotted with σ_P as the

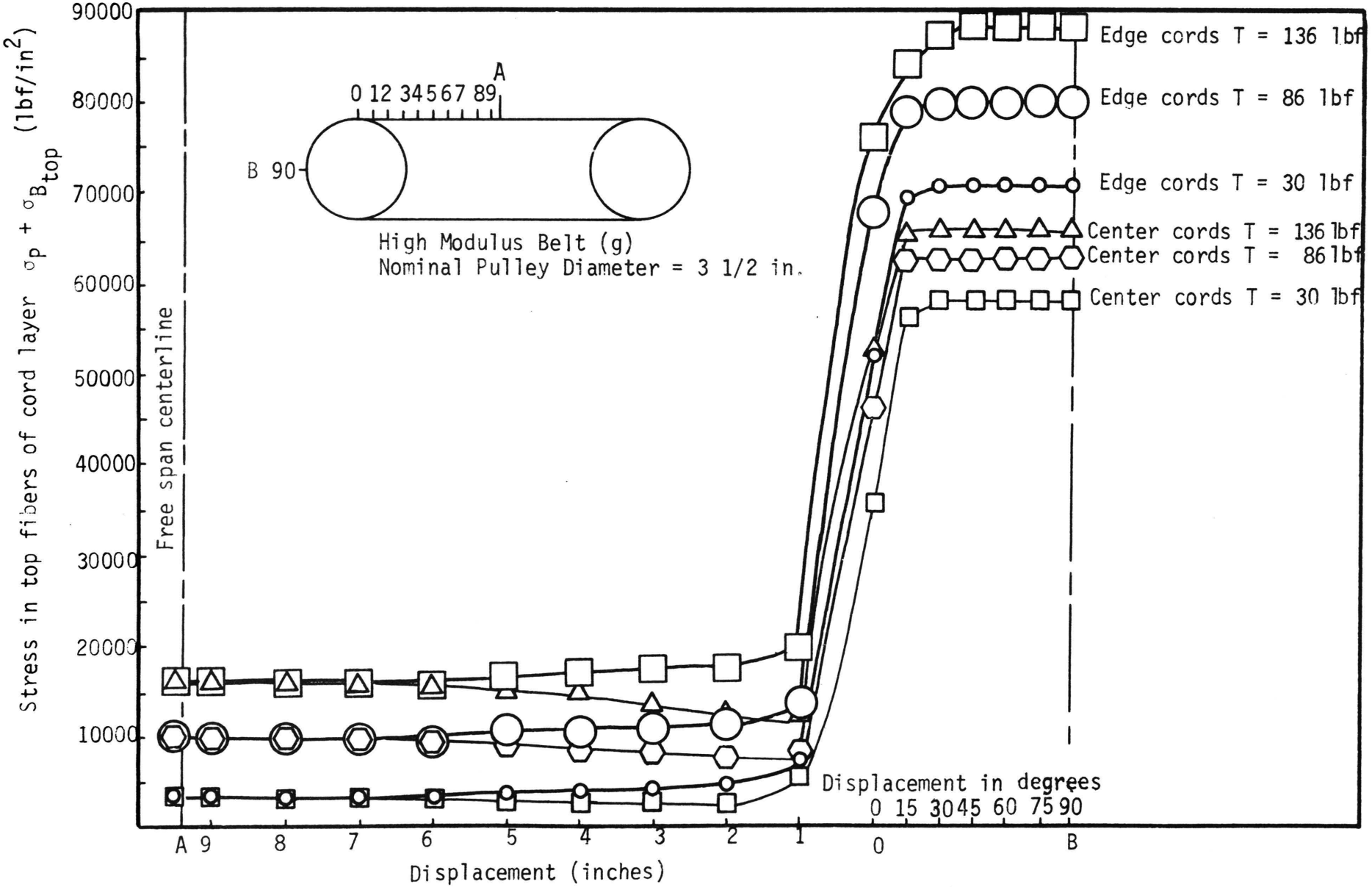

Figure 6.1. Symmetric Quarter of Statically Loaded Bending Cycle

abscissa and $\left(\sigma_P + \sigma_{B_{top}}\right)/\sigma_P$ as the ordinate for all the test runs. This method of plotting allows relative magnitude comparison between the stresses endured in the span and those endured in the wrap on an unloaded drive. For normal preloads on the high modulus belt, maximum center cord wrap stresses range from 3.5 to 16 times the preload stress while edge cord wrap stresses take on 4 to 24 times the static preload value. For the low modulus belt, maximum center wrap stress was 2 to 7 times the preload stress, and maximum edge wrap stress varied from 2.8 to 7.5 times the preload stress.

An observation based on the curves shown in Figures 6.2 and 6.3 is that as preload increases, a higher percentage of the total stress load is carried by the edge cords. This fact is even evident in the free span as shown by Figure 6.1. For increasing preloads, there is a greater redistribution of center and edge stresses as the belt approaches the pulley sheave with the edge cords always carrying the higher stress load.

The graphs in Figures 6.4 through 6.9 illustrate the application of the bending strain and preload strain calculations to Equations 3.13 through 3.21 in order to determine the position of the neutral axis and the elevation of zero stress in the cord layer. The basic assumption made in these equations is that bending stress varies linearly in the radial direction and load stress is uniformly distributed in the radial direction through the cord layer.

The error involved in the determination of the neutral axis with respect to the top of the cord layer in this report is shown in the following analysis. The basic equation for the distance from the

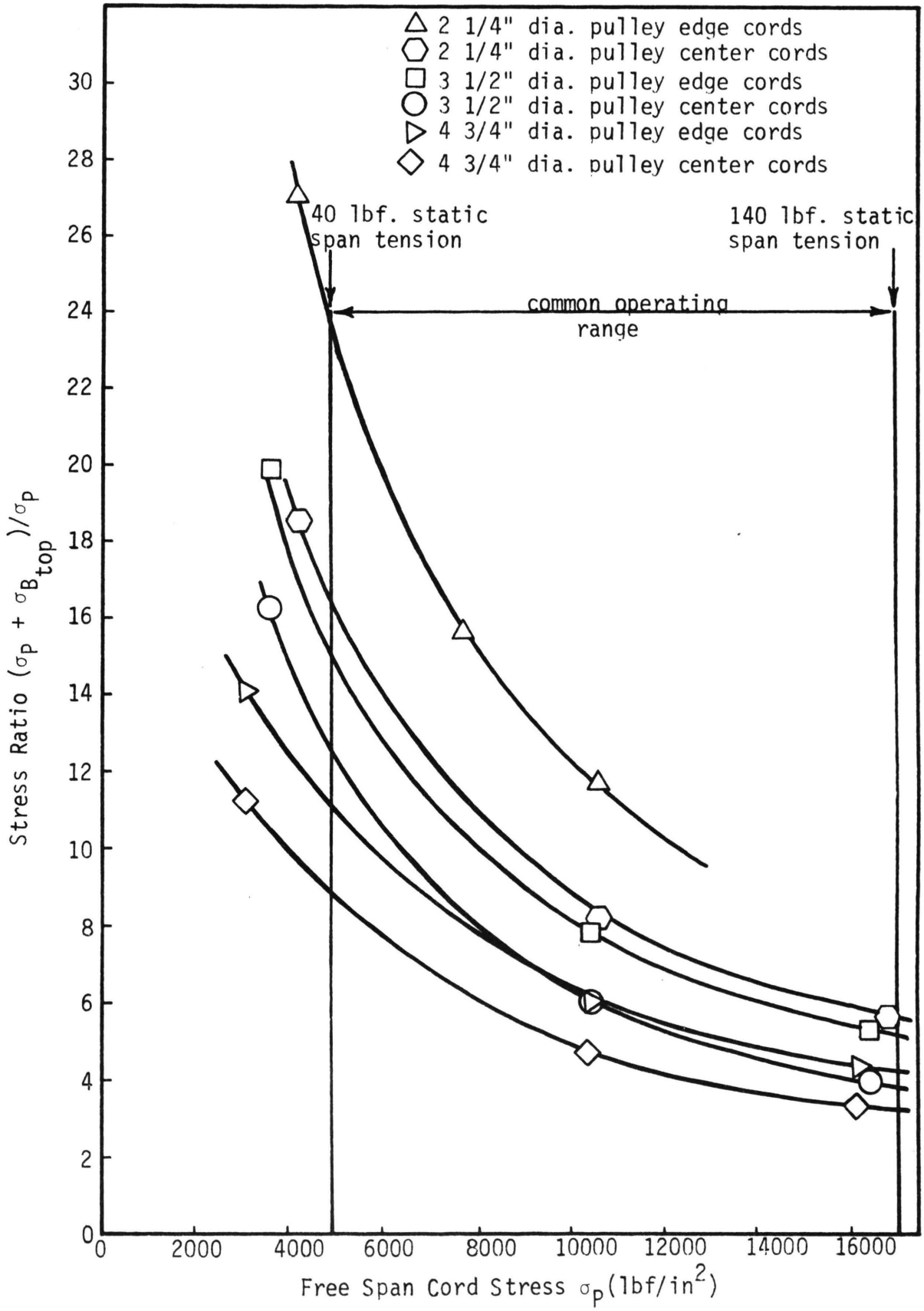

Figure 6.2. The Effect of Bending Stress on the Top Fibers in the Cord Layer of the High Modulus Test Belt (g)

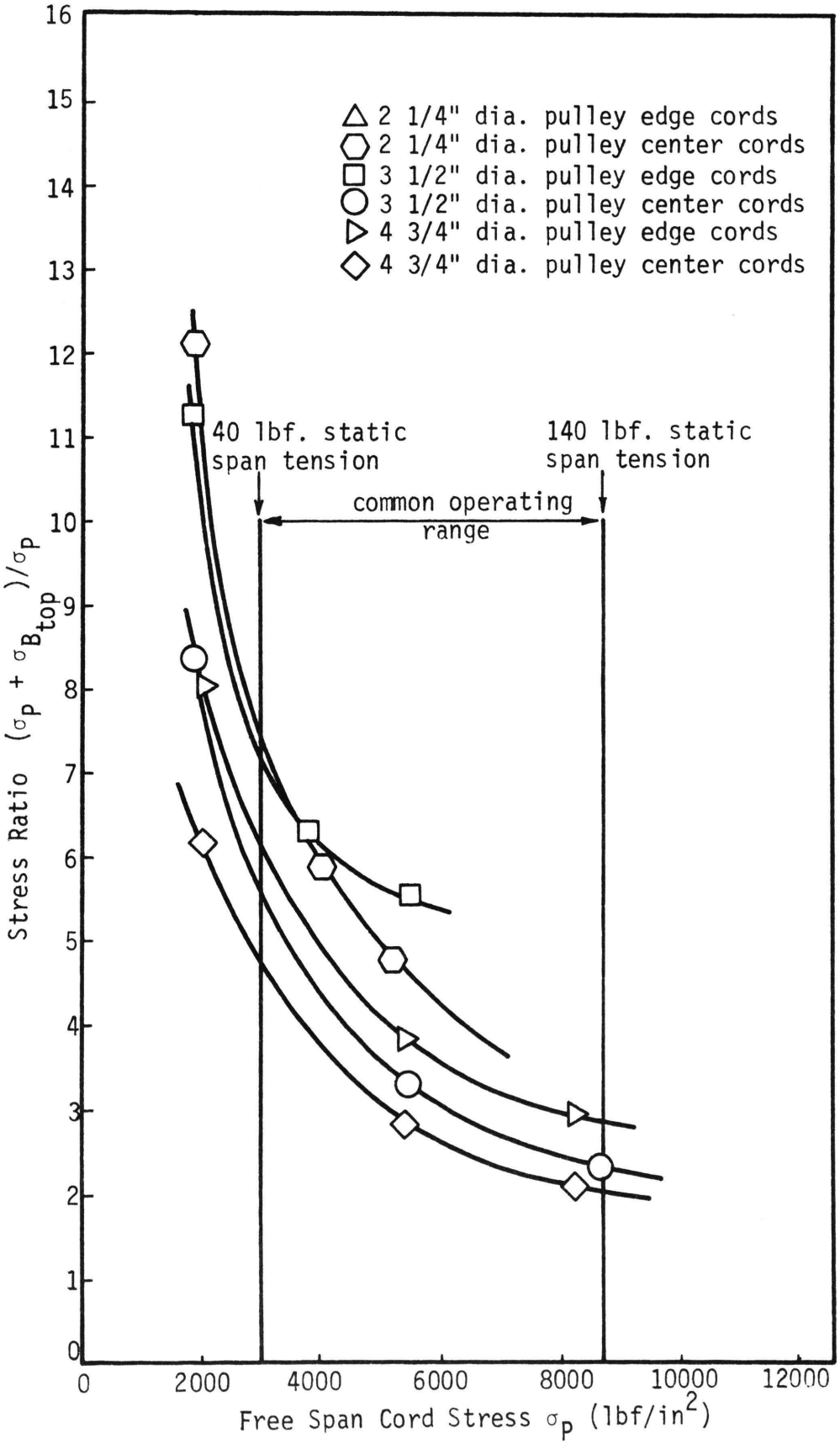

Figure 6.3. The Effect of Bending Stress on the Top Fibers in the Cord Layer of the Low Modulus

neutral axis to the cord top is

$$e_{top} = \frac{S\ \varepsilon_{B_{top}}}{1 + \varepsilon_{B_{top}}} \tag{6.6}$$

For small deviations in the quantities S and $\varepsilon_{B_{top}}$, the error involved in this computation is δe_{top}.

$$\delta e_{top} = \left(\frac{\partial e_{top}}{\partial S}\right) \delta S + \left(\frac{\partial e_{top}}{\partial \varepsilon_{B_{top}}}\right) \delta \varepsilon_{B_{top}} \tag{6.7}$$

$$\delta e_{top} = \left(\frac{B_{top}}{1 + \varepsilon_{B_{top}}}\right) \delta S + \left(\frac{S}{1 + \varepsilon_{B_{top}}^{2}}\right) \delta \varepsilon_{B} \tag{6.8}$$

The maximum numerical value of Equation 6.8 is computed for the equipment used

$$\delta e_{top} = \left(\frac{.03}{1.03}\right)\left(\frac{1}{64}\right) + \left(\frac{2.375}{(1.03)^2}\right) (.000020) \tag{6.9}$$

$$\delta e_{top} = 0.000499 \text{ inches} \tag{6.10}$$

The maximum error in computing a top cord elevation in a cord .037 inches in diameter would be less than 1.4% and for a cord 0.055 inches in diameter, it would be less than 1.0%. The error analysis may also be extended to the calculation of zero stress elevation. The expression for the elevation of zero stress may be written as

$$e_z = -e_{top}\left(\frac{\varepsilon_P}{\varepsilon_{B_{top}}}\right) \tag{6.11}$$

The corresponding error expression is

$$\delta e_z = \left(\frac{\partial e_z}{\partial e_{top}}\right)\delta e_{top} + \left(\frac{\partial e_z}{\partial \varepsilon_P}\right)\delta\varepsilon_P + \left(\frac{\partial e_z}{\partial \varepsilon_B}\right)\delta\varepsilon_B \tag{6.12}$$

$$\delta e_z = \left(-\frac{\varepsilon_P}{\varepsilon_{B_{top}}}\right)\delta e_{top} + \left(-\frac{e_{top}}{\varepsilon_{B_{top}}}\right)\delta\varepsilon_P + \left(\frac{e_{top}\,\varepsilon_P}{\varepsilon_B^{\,2}}\right)\delta\varepsilon_B \tag{6.13}$$

Inserting maximum deviations for all quantities, one obtains

$$\delta e_z = \left|\left(-\frac{.005}{.010}\right)(.0005)\right| + \left|\left(-\frac{.025}{.010}\right)(.000010)\right| + \left|\frac{(.025)(.005)}{(.010)^2}\,(.000020)\right| \tag{6.14}$$

$$\delta e_z = 0.0003 \text{ inches}$$

Placement of the elevation of zero stress within .0003 inches in a cord of diameter .037 represents less than 1% error in accuracy and in the .055 diameter cord less than 0.6% error. The thickness of the strain gages was also identified as a source of error because it is possible that the gages measure strain at a radius slightly greater than the top elevation of the cords. The thickness of a gage was measured and it was determined that the center of the gage lay about 0.00125 inches above the top of the cords. The total error

in determining the elevation of the neutral axis and elevation of zero stress would still be less than 0.002 inches which represents error in the range of 5.4% on the high modulus 0.037 inch diameter cord and 3.6% on the low modulus .055 inch diameter cord.

Each of the graphs in Figures 6.4 through 6.9 is plotted for a single pulley size and belt cord. Preload versus cord elevation axes allow the presentation of four sets of points on each graph. The neutral axis lines represent the elevation in the cord layer where cord stress is equal to the uniformly distributed preload stress. The zero stress lines represent the elevation in the cord where the interaction of compressive bending and tensile preload stress yields zero stress in the tangential direction. Below the line of zero stress the belt cords are in compression. The points on each graph in Figures 6.4 through 6.9 can be projected back to the cord cross section on the left to obtain their relative physical significance. Because the edge gages always registered higher values of $\left(\varepsilon_{tot_i} - \varepsilon_{P_i}\right)$ than the center gages, the edge cord neutral axis was always calculated to be lower in the cord cross section. An accurate measurement of the concavity of the top surface of the cord layer as shown in Figure 6.10 would have established the absolute elevation of the neutral axis with respect to the pulley axis. This measurement would allow the determination of the neutral axis variation in the radial direction across the concave cord layer. The present analysis considers only the location of the neutral axis with respect to the top surface of the cord layer and does not compute its location with respect to the absolute axial direction. Present data has, however, permitted the

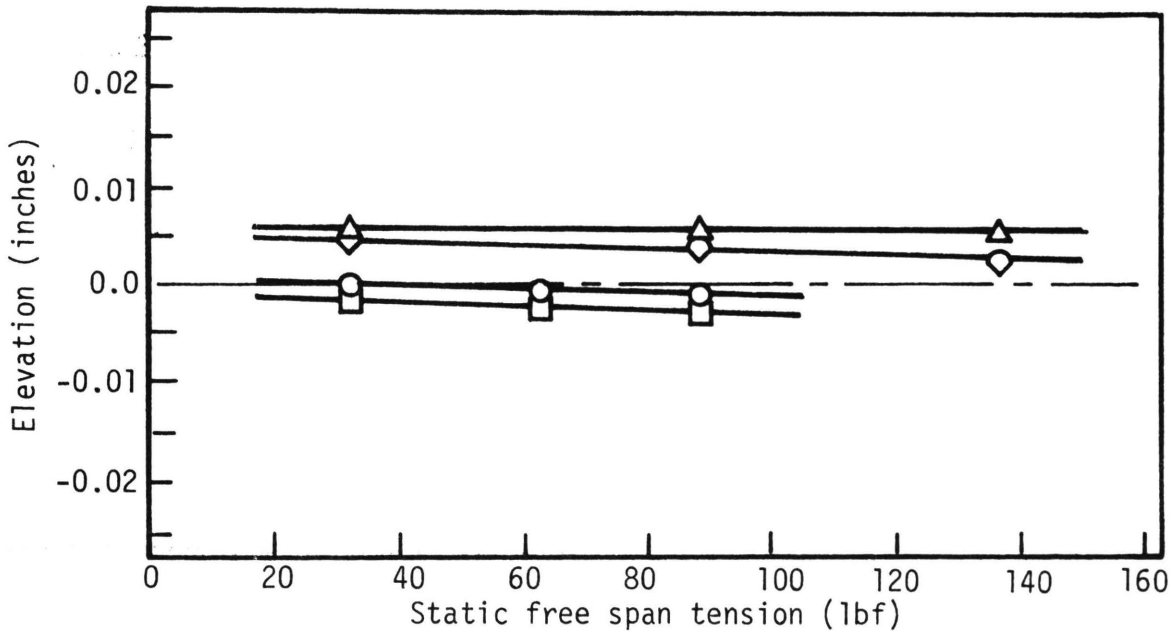

Figure 6.4. Neutral Axis and Zero Stress Elevation
High Modulus Cords (g), 2 1/4 inch pulley

Symbols for both Figures:
△ Neutral axis of center cords
◇ Elevation of zero stress -- center
○ Neutral axis of edge cords
□ Elevation of zero stress -- edge

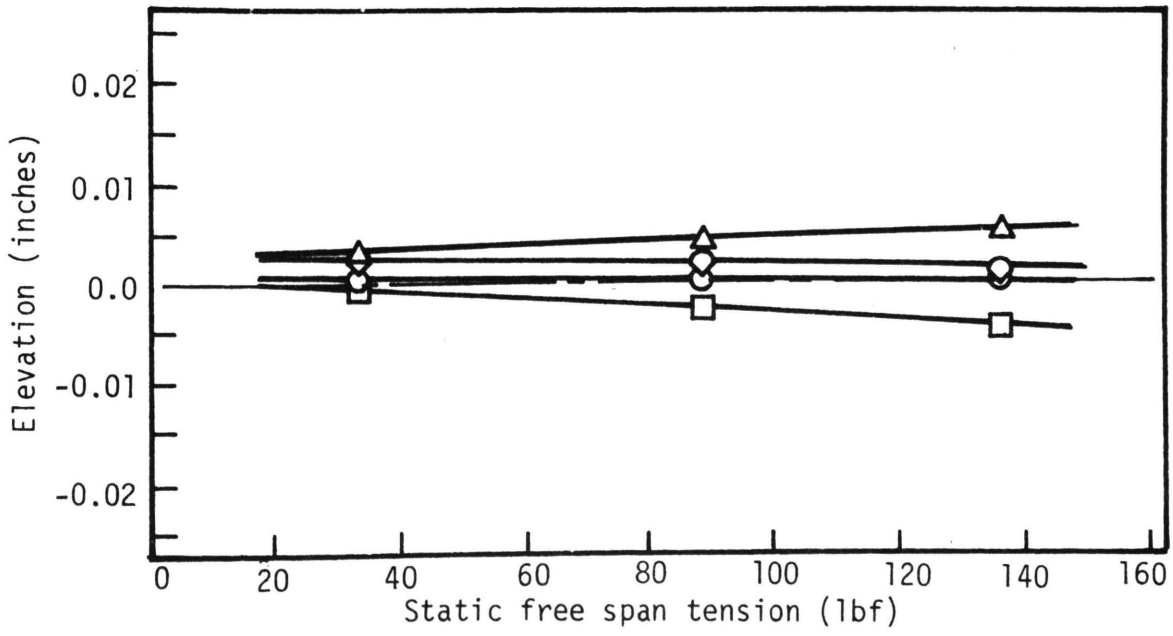

Figure 6.5. Neutral Axis and Zero Stress Elevation
High Modulus Cords (g), 3 1/2 inch pulley

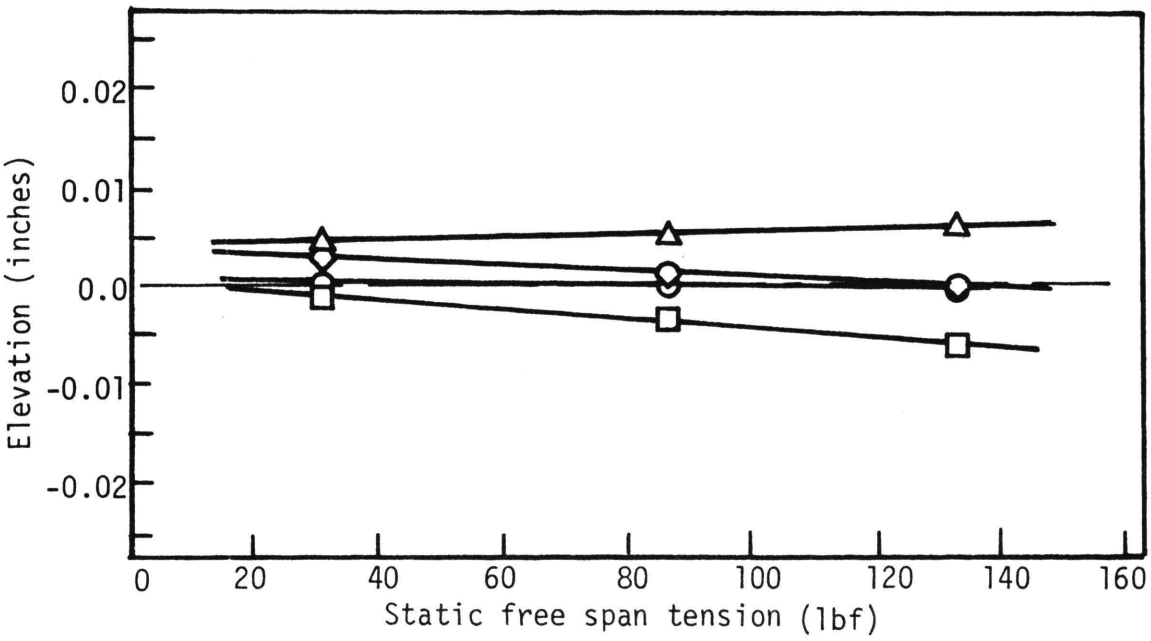

Figure 6.6. Neutral Axis and Zero Stress Elevation
High Modulus Cords (g), 4 3/4 inch pulley

Symbols for both Figures:
△ Neutral axis of center cords
◇ Elevation of zero stress -- center
○ Neutral axis of edge cords
□ Elevation of zero stress -- edge

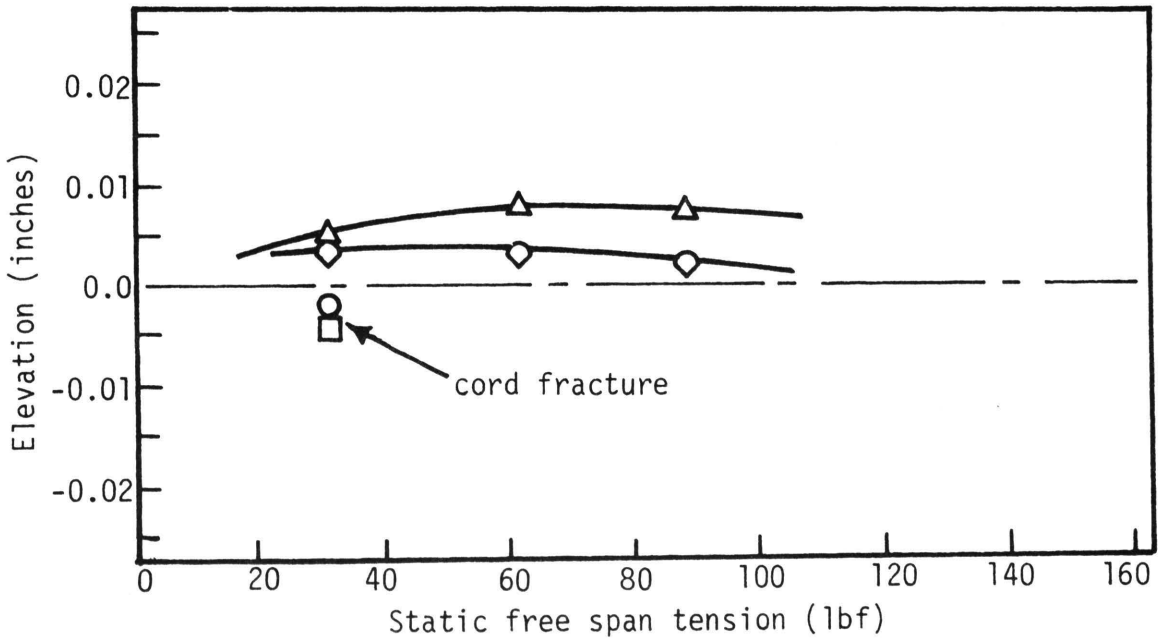

Figure 6.7. Neutral Axis and Zero Stress Elevation
Low Modulus Cords (h), 2 1/4 inch pulley

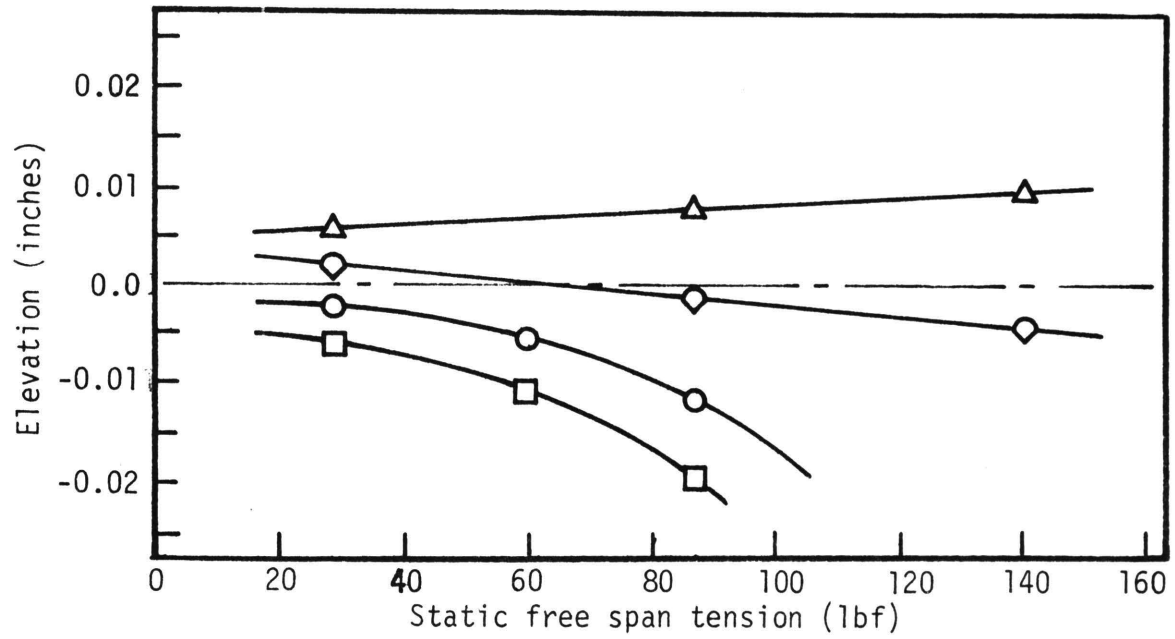

Figure 6.8. Neutral Axis and Zero Stress Elevation
Low Modulus Cords (h), 3 1/2 inch pulley

Symbols for both Figures:
△ Neutral axis of center cords
◇ Elevation of zero stress -- center
○ Neutral axis of edge cords
□ Elevation of zero stress -- edge

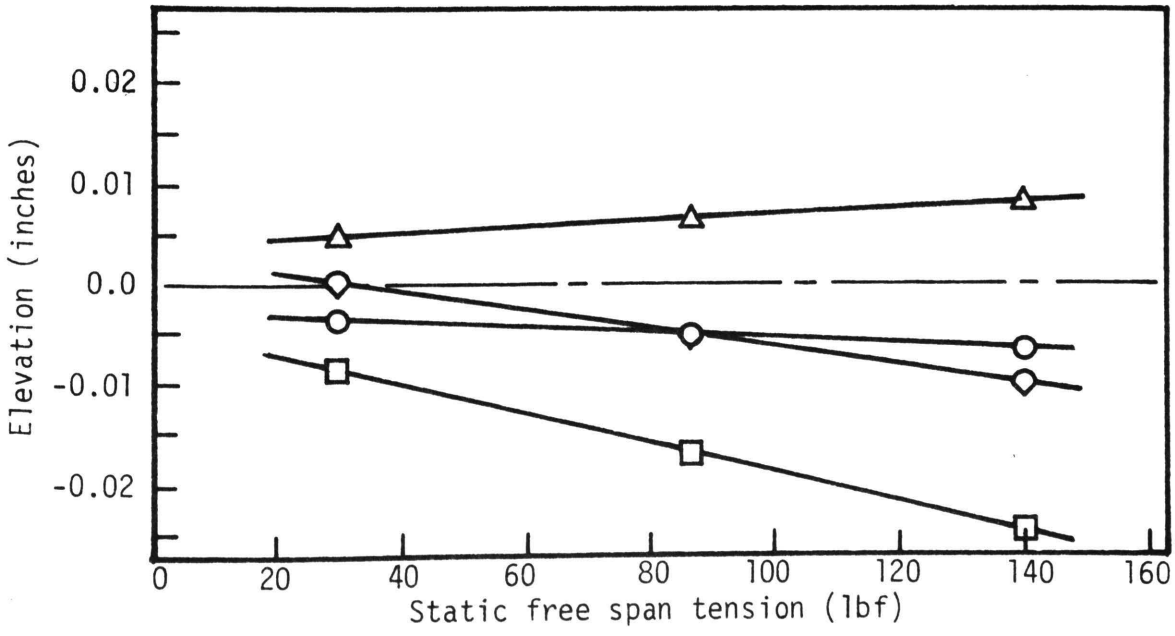

Figure 6.9. Neutral Axis and Zero Stress Elevation
Low Modulus Cords (h), 4 3/4 inch pulley

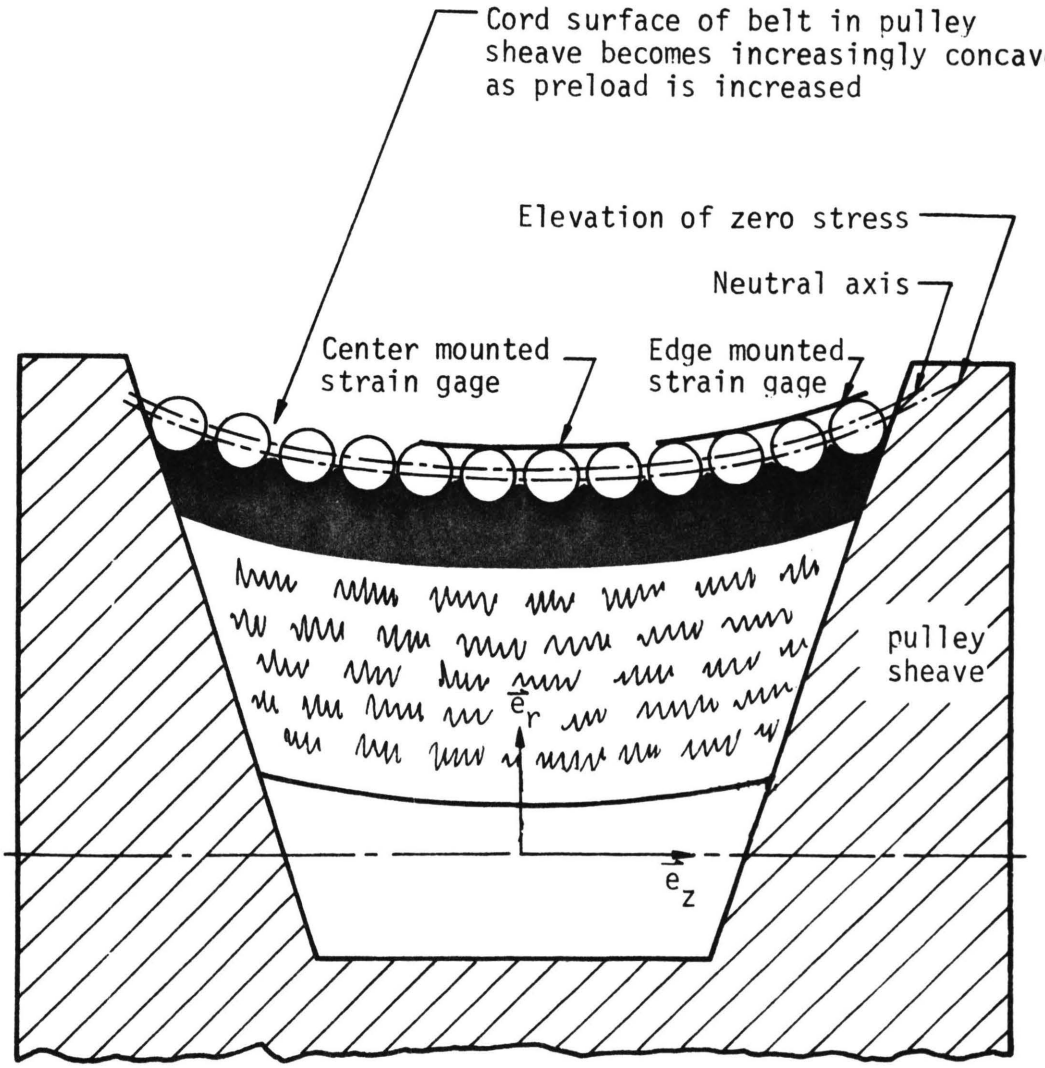

Figure 6.10. Cross Section of High Modulus Exposed Cord V-belt in Pulley Sheave

calculation of maximum tensile strain, maximum compressive strain, and therefore, the linear profile of strains radially across center and edge cords.

Finally, the bending stress analysis establishes the existence of tensile and compressive stresses within the cord layer. Compressive stresses have not been calculated because the compressive moduli of the belts tested were not known. Compressive strains in the cord layer, however, can be calculated using Equation 3.22. Maximum compressive strains were generally only slightly less than maximum tensile strains in the high modulus belt where the elevation of zero stress was very near the geometric cord center. On the low modulus belt, maximum compressive strains were much lower than maximum tensile strains due to the low elevation of the zero stress level as shown in Figures 6.7, 6.8, and 6.9. The existence of high tensile and compressive strains in v-belt cords alluded to by Johnson and Hornung [9] has been established by this analysis. Because belt cords are made of entwined strands of fiber, a single strand may experience a change from tension to compression within a very short distance. The cyclic loads used in a refined fatigue analysis might then include compressive and tensile values since each cord strand experiences both types of loading at different points along its length.

B. CENTRIFUGAL STRESS DETERMINATION

Figure 6.11 has been drawn to demonstrate the variation of centrifugal stress in the high modulus belt as calculated from Equation 3.9. Similar curves for the low modulus belt would give

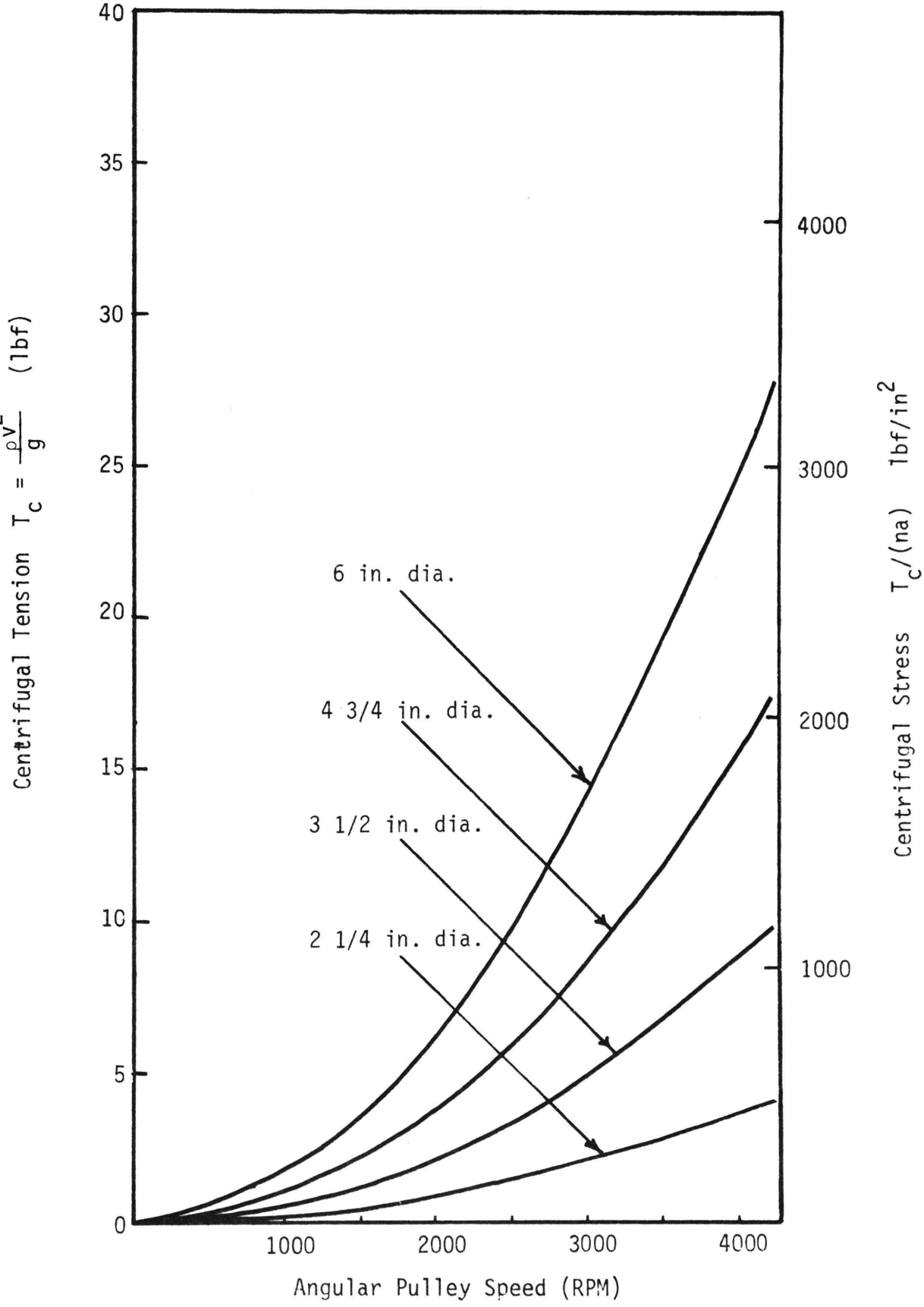

Figure 6.11. Centrifugal Stress Variation in High Modulus Belt (g)

slightly higher centrifugal tensions due to the fact that the low modulus belt is slightly heavier. Centrifugal effects are usually quite small, but since the centrifugal tension varies as the square of the linear belt velocity, large pulley diameters and high rotation rates produce significant values of centrifugal stress. Graphical presentation of Equation 3.9 permits an order of magnitude comparison of centrifugal stress and the other belt stress components. It is seen that for the experiment under discussion, centrifugal stress never exceeded 13, 7, and 3 pounds per side on the 4 3/4, 3 1/2, and 2 1/4 inch diameter pulleys, respectively, at 3,600 RPM. A minimum preload of 30 pounds per side is still larger than the largest centrifugal tension, but the superposition of centrifugal effects on span tension alter tension enough to warrant their calculation.

C. RESULTS OF DYNAMIC STRESS ANALYSIS

The next phase of this study was the determination of cord load stress variations over driver and driven pulleys in the dynamic torque loaded state. It was hoped that total dynamic stress could be computed and then bending and centrifugal effects could be subtracted from the total to yield load stress variation around the pulleys. As described in Section IV, attempts to measure dynamic strain were made with a high speed photography system and a magnetic pickoff system. Both methods failed to yield meaningful results, but the information obtained by this study should be helpful in defining a more precise photographic strain measuring system for future experimentation. The analytical model of load tension

variation presented by Hornung [7] was used to complete the present analysis.

1. PHOTOGRAPHIC STRESS STUDY RESULTS

The results of the photographic effort are shown in Figures 6.12 and 6.13. Synchronization of the camera shutter and strobe flash on a single marked section of moving belt was easily accomplished with the flash delay and photoelectric pickoff. The 3.0 microsecond film exposure caused by a single strobe pulse was sufficient to give a sharp image of the belt at speeds of 500 to 1,000 inches per second as shown in Figure 6.12. The results of photographing a static section of belt in the free span under carefully controlled preload conditions are shown in Figure 6.13. The negatives of these photographic prints were placed on the table of an overhead projector and projected to a smooth white vertical surface against a wall. A cathometer placed approximately 8 feet from the wall was focused on the image of the marked belt section. The quality of the calibrated marks on the projected image was such that changes of less than one percent in displacement could not be observed. Suggestions for possible improvement of the photographic technique are discussed in the conclusions section of this report.

2. MAGNETIC PICKOFF-TIMER SYSTEM RESULTS

Measurements taken with the magnetic pickoff also produced no presentable results. Readings were consistent to within one percent when the pickoff was focused on a given portion of the belt drive. There is, however, a fundamental theoretical problem associated with trying to discern the difference in the time of passage of two thin staples and relating this time differential to a stress variation.

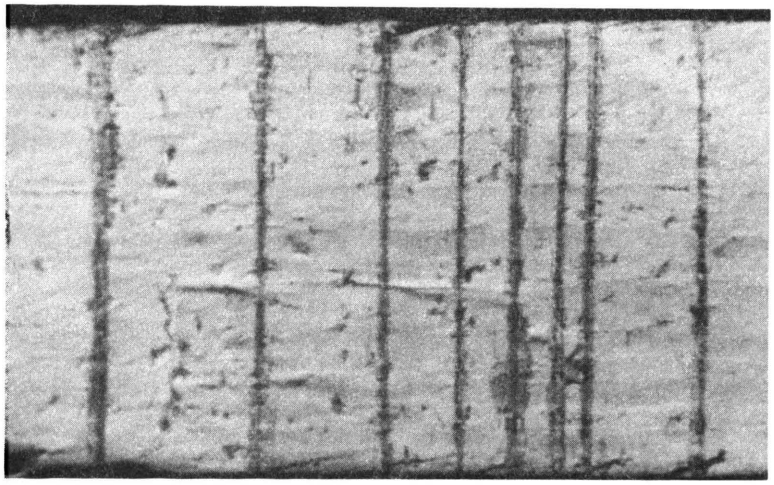

658 in/sec on 4 3/4 in. Diameter Pulley

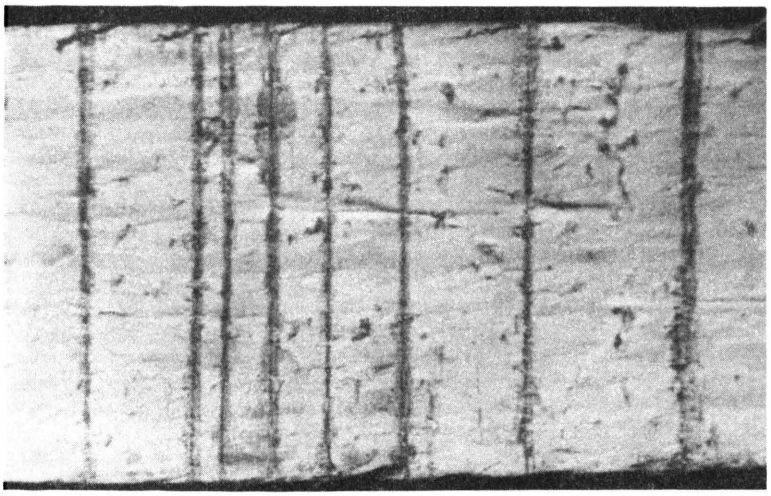

679 in/sec on 4 3/4 in. Diameter Pulley

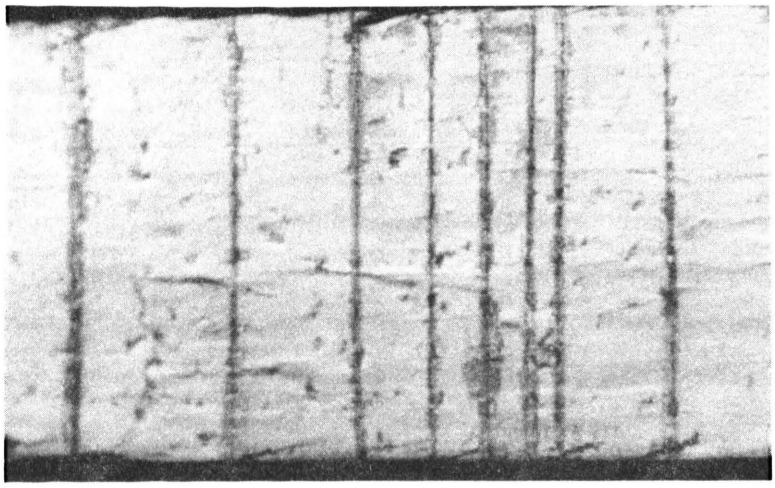

753 in/sec on 4 3/4 in. Diameter Pulley

Figure 6.12. Time Synchronized Photographs of a Marked Belt Section Traveling over a 4 3/4 inch diameter v-pulley

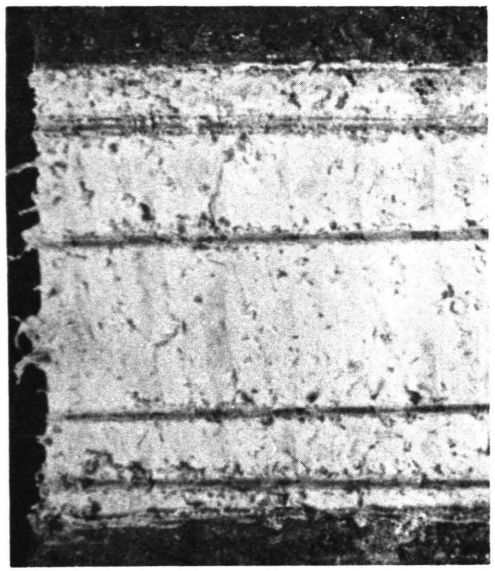

Belt Tension 5 lbf

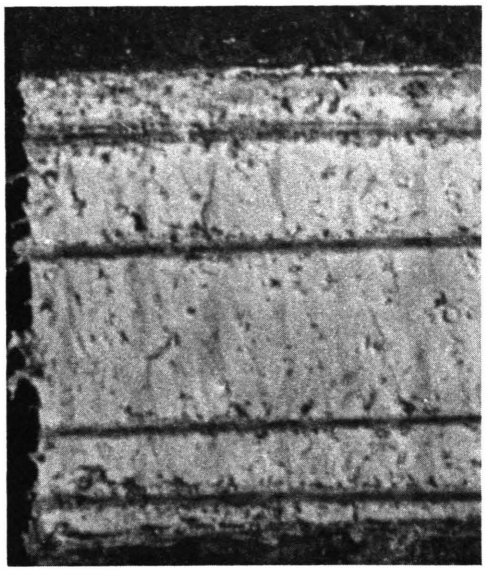

Belt Tension 104 lbf

Belt Tension 166 lbf

Photographs 6x life size

Figure 6.13. Three Static Photographs Showing Marked Section of Exposed Cord Layer on Low Modulus Belt (h)

Two staples in the belt could be considered to mark off a belt segment of constant mass rather than of constant length. If the belt is subjected to the conditions of constant mass rate, any strain in a constant mass segment will be accompanied by an equal percentage increase in velocity in order that the mass flow rate of the belt remains constant. Hence, the relative consistency in readings obtained for positions around the pulley wrap might be due to the constant mass rate of the belt.

The test run which determined the time of passage of a solid quarter inch staple as described in Section V was attempted next. The solid staple fixed a constant length transducing section as opposed to the constant mass section prescribed by the two thin staples. The wide staple, however, stiffened the whole belt section where it was located. Discrepancies in readings obtained by this method may have been due to the fact that the altered belt properties of the fixed length section caused inconsistencies in the slip motion and shear of the belt as it passed around the pulleys. Data from the magnetic pickoff-timer system then led to no conclusive results.

3. RESULTS OF ANALYTICAL LOAD STRESS DETERMINATION

In order to complete the determination of the total stress in automotive v-belts, the Hornung analytical solution for belt tension variation due to torque load was employed. Twenty drive situations were simulated by a digital computer using a proprietary program supplied by the Dayco Corporation. Drives employing the 2 1/4, 3 1/2, and 4 3/4 inch diameter pulley sizes were simulated for the high modulus belt. Torque loads varying from 5 to 10 pound feet

were used with total preloads, $\left(T_1 + T_2\right)$, between 125 and 225 pounds. The results of these runs are shown in Figures 6.14 through 6.16. The Hornung analysis generates only a value of load tension, hence stress distributions in the radial and axial directions and shear forces are ignored. The analysis does, however, incorporate several important characteristics of belt power transmission. In each drive situation, Figures 6.14 through 6.16, the tension variation does not necessarily occupy the entire contact angle. So-called adhesion zones or inactive arcs in which no tension variation occurs are found on the entrance side of both driver and driven pulleys. The inactive arc on the driver pulley is always longer than that on the driven. An overloaded belt drive is characterized by an active arc equal to the entire contact angle while at the end of the contact angle the belt tension fails to reach the tight-side tension again. Several overloaded runs are shown in Figures 6.14 and 6.15 where the tight side tension has not developed at position π on the driven pulley. The commonly observed fact that increasing load causes a belt to slip first on the driven pulley is accounted for by the Hornung analysis.

If load stress were considered as being uniformly distributed across the cord layer, the stress levels indicated on the right edge in Figures 6.14 through 6.16 would be valid. Even if the edge cords carry one to two times the load stress in the center cords as determined by Gerbert [5], the cyclic stress variation due to torque load constitutes only a small superposition on the maximum bending stress. The load stress varies at a relatively slow rate compared

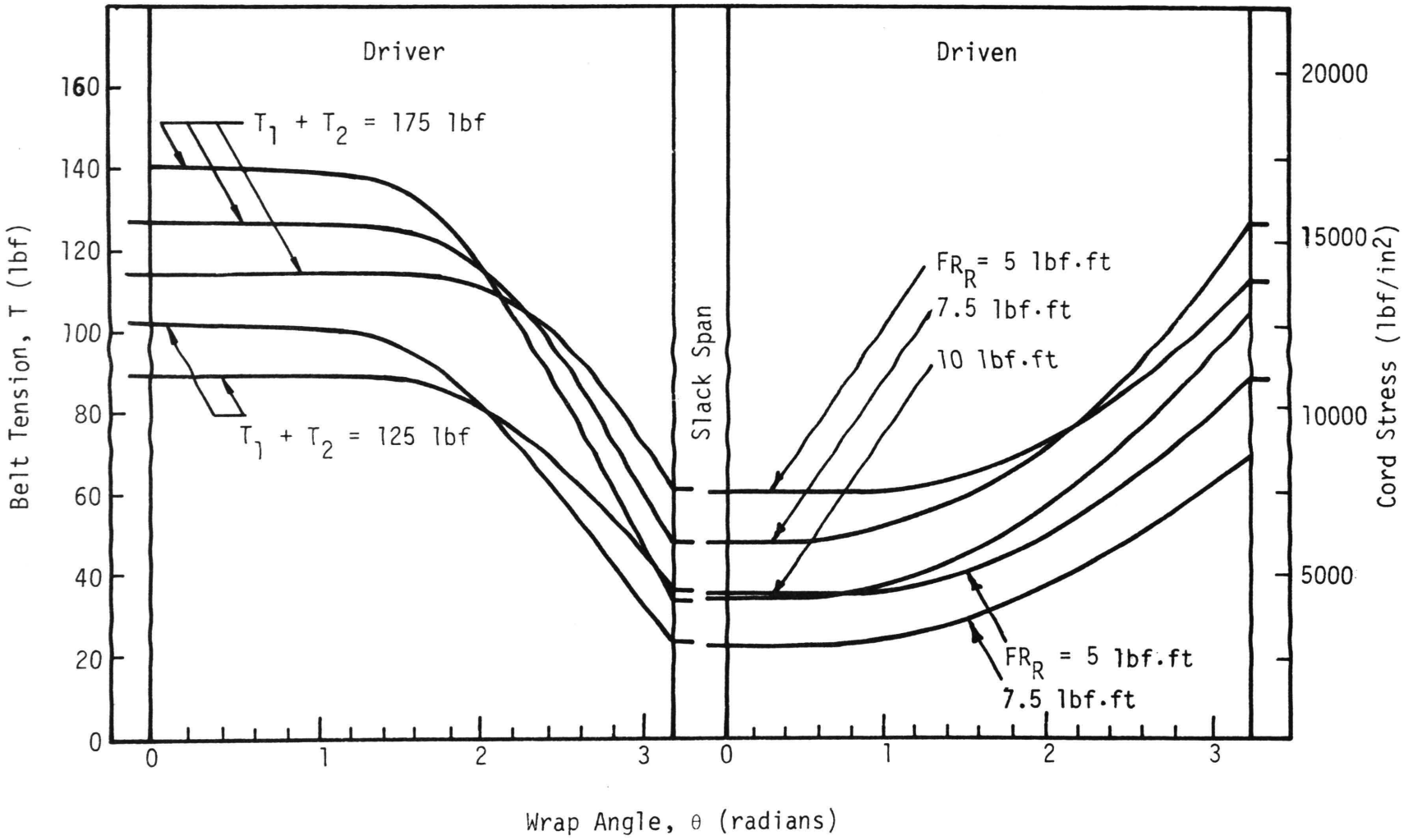

Figure 6.14. Hornung Load Tension Variations -- High Modulus Belt (g) on two 2 1/4 inch pulleys

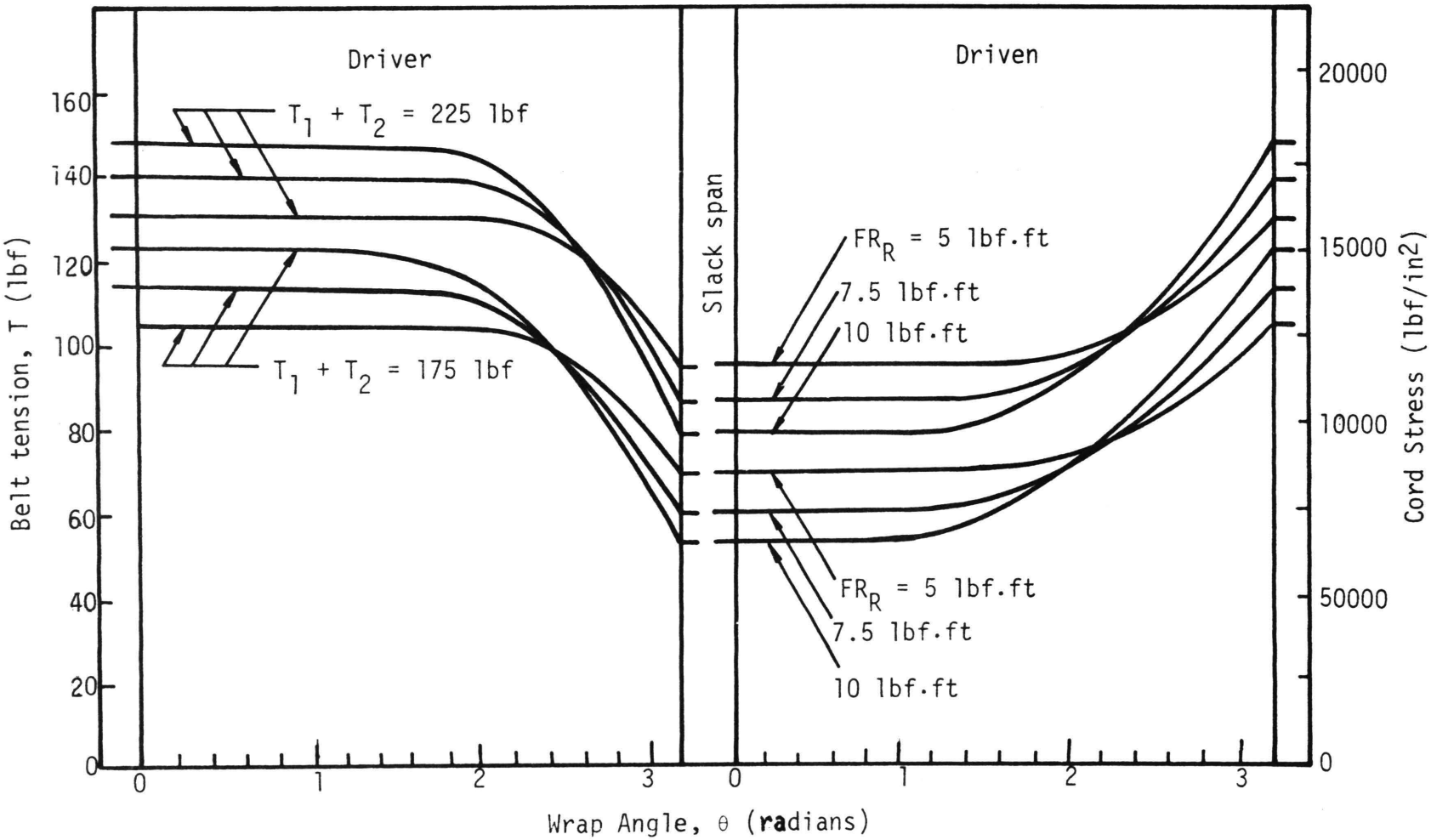

Figure 6.15. Hornung Load Tension Variation -- High Modulus Belt (g) on two 3 1/2 inch pulleys

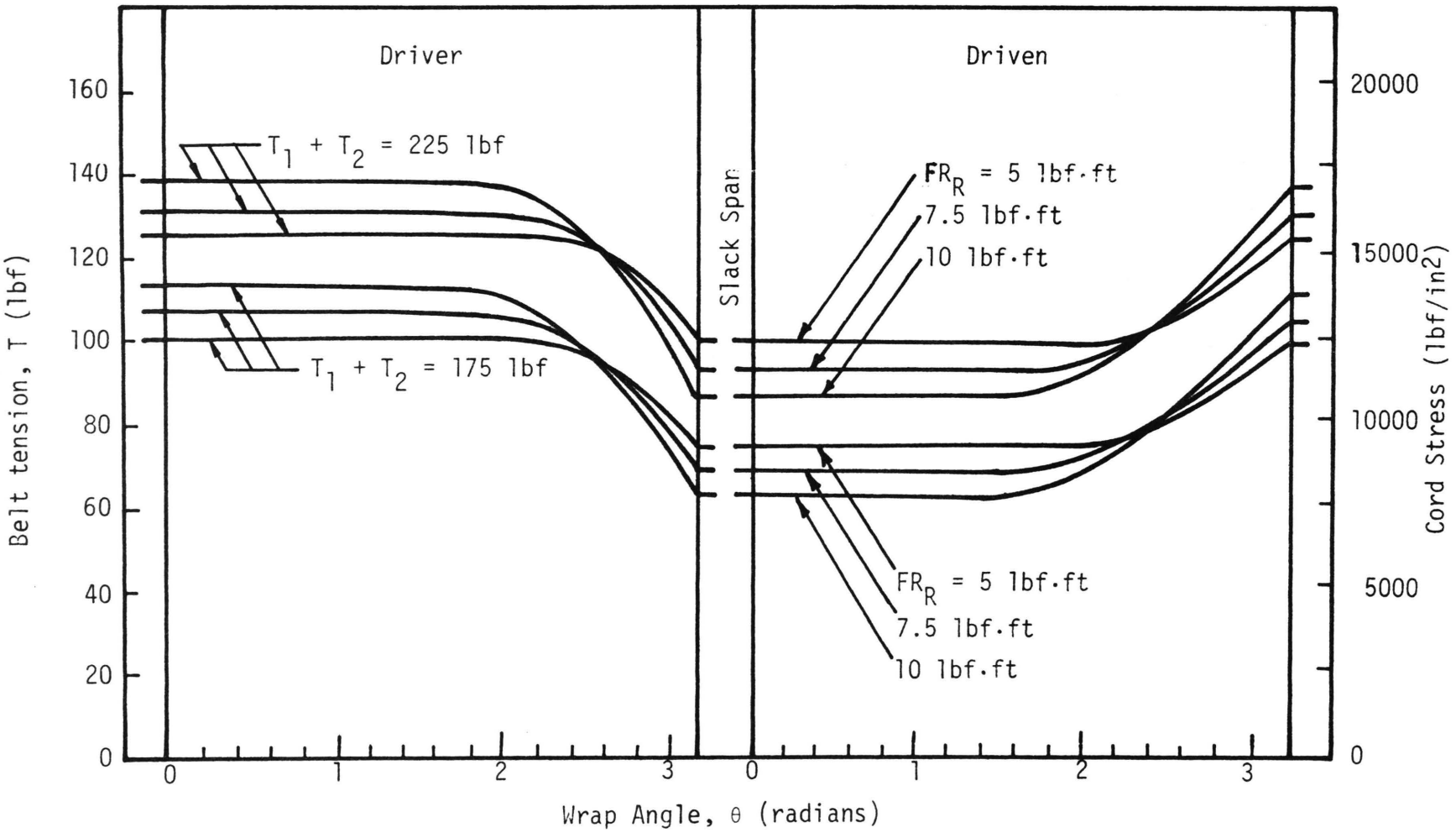

Figure 6.16. Hornung Load Tension Variation -- High Modulus Belt (g) on two 4 3/4 inch pulleys

to the abrupt changes in bending stress on the top of the cord layer as the belt enters and leaves the pulley sheave. The Hornung analysis contributes a logical yet simplified analysis of load tension variation. It is important for its calculation of active and inactive arc lengths and its consideration of wedging forces.

D. COMPARISON OF STRESS COMPONENTS IN AUTOMOTIVE RANGE BELT DRIVES

This report has determined all types of tangential belt stress in a set of automotive type drives. Bending, centrifugal, preload and torque load stresses varied substantially over the parameter ranges considered here, but a definite hierarchy in importance of effects is readily observable. Bending stress in the top of the cord layer is by far the highest stress endured by the v-belt. Since bending strain is most strongly influenced by geometry, bending stress was much higher in the high modulus cords than it was in the low modulus belt cords. Bending also causes both tensile and compressive stresses in the belt cords. The next largest stress consideration would be load stress. This stress can be considered as a constant stress equal to the slack side tension with a superimposed cyclic value representing its increase to the tight side tension over the driver pulley. Centrifugal stress is the smallest stress component in automotive drives. It is constant in nature because it depends only on belt speed and belt weight. It is important, however, because in a fixed centers drive, centrifugal stress causes the belt to ride outward radially in the pulley sheave due to the effect of uniformly increasing the length of the whole belt.

The culmination of the present belt stress analysis is a superimposing of all the stress components in a given belt drive by

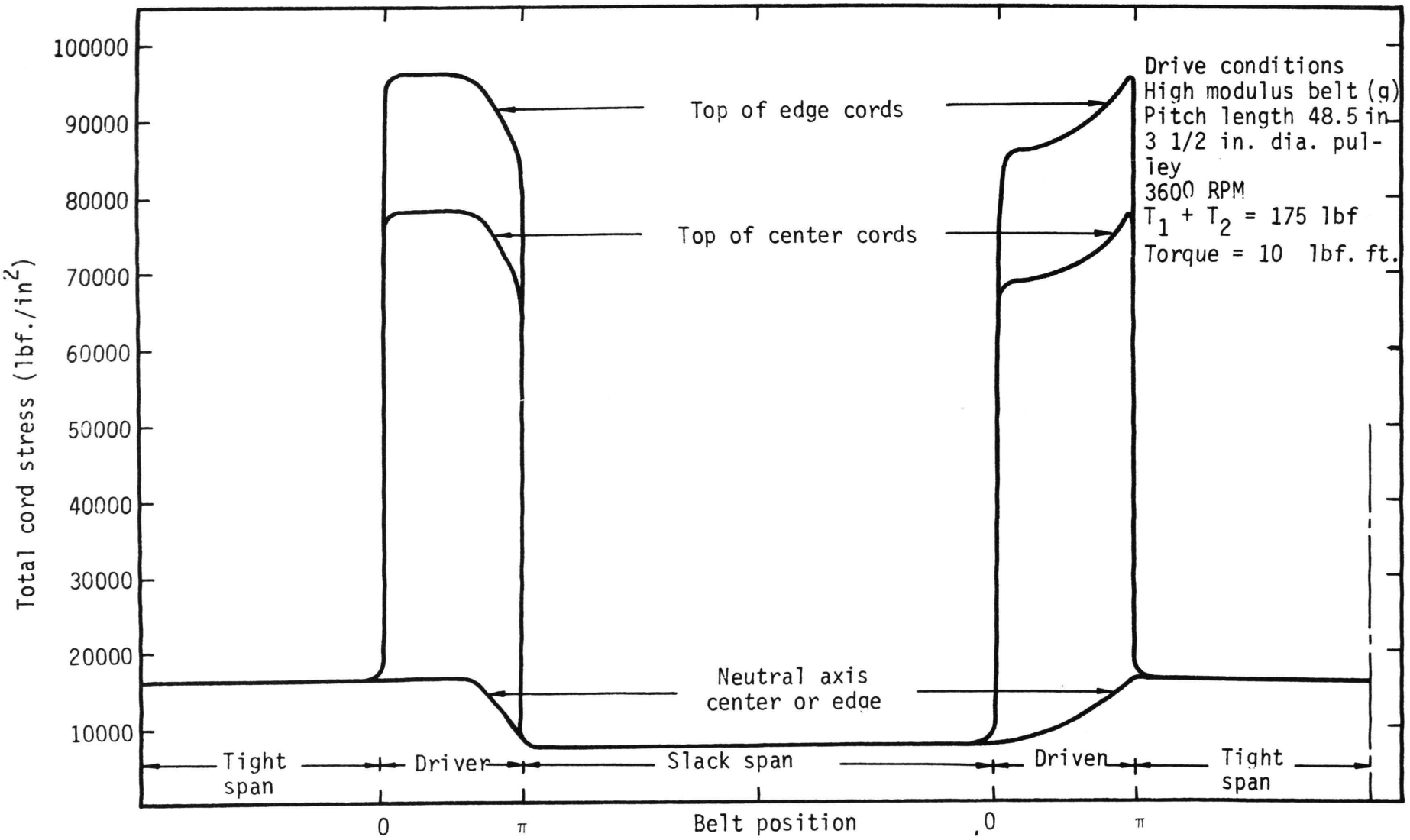

Figure 6.17. Superposition of Load, Centrifugal, and Bending Stress for a Specific Set of Drive Parameters

the use of Equation 3.23. This equation can be applied locally to any point in the cord layer because the bending stress term may be written for any radial elevation or axial position. Figure 6.17 indicates the tensile cord stress cycle found in the top elevation of the center and edge cords and at the neutral axis of a v-belt for a specified drive situation. The versatility of separating belt stress components and then superimposing their individual effects to obtain a complete picture of belt stress is illustrated by Figure 6.17. A measurement of total stress on a dynamic torque loaded drive would indicate the validity of the present analysis and possibly demonstrate any coupling effects between stress components and dynamic drive parameters. This was the purpose of the photographic stress tests. Hence, photographic stress measurements accomplished in future tests will provide an interesting check on the present work.

E. RESULTS OF EXPERIMENTAL POWER LOSS DETERMINATION

The final method of dynamic analysis was the comparison of percentage speed loss with traction coefficients for the drive situations studied in this analysis as described in Equations 3.25 and 3.31. The highest quality curves were obtained from test runs on the 2 1/4 inch diameter pulleys because traction coefficients of nearly .90 were obtainable while speed losses ranged from zero to eight percent (Figures 6.18, 6.19, and 6.20). The maximum traction coefficient obtainable on the 3 1/2 inch diameter pulley was .58 and on the 4 3/4 inch diameter pulley, it was .42. Speed loss was in all cases below 1.5 percent on the 3 1/2 and 4 3/4 inch diameter pulleys so that the .25% error of the tachometer was a significant factor in causing the poor appearance of Figures 6.21 through 6.24 as compared

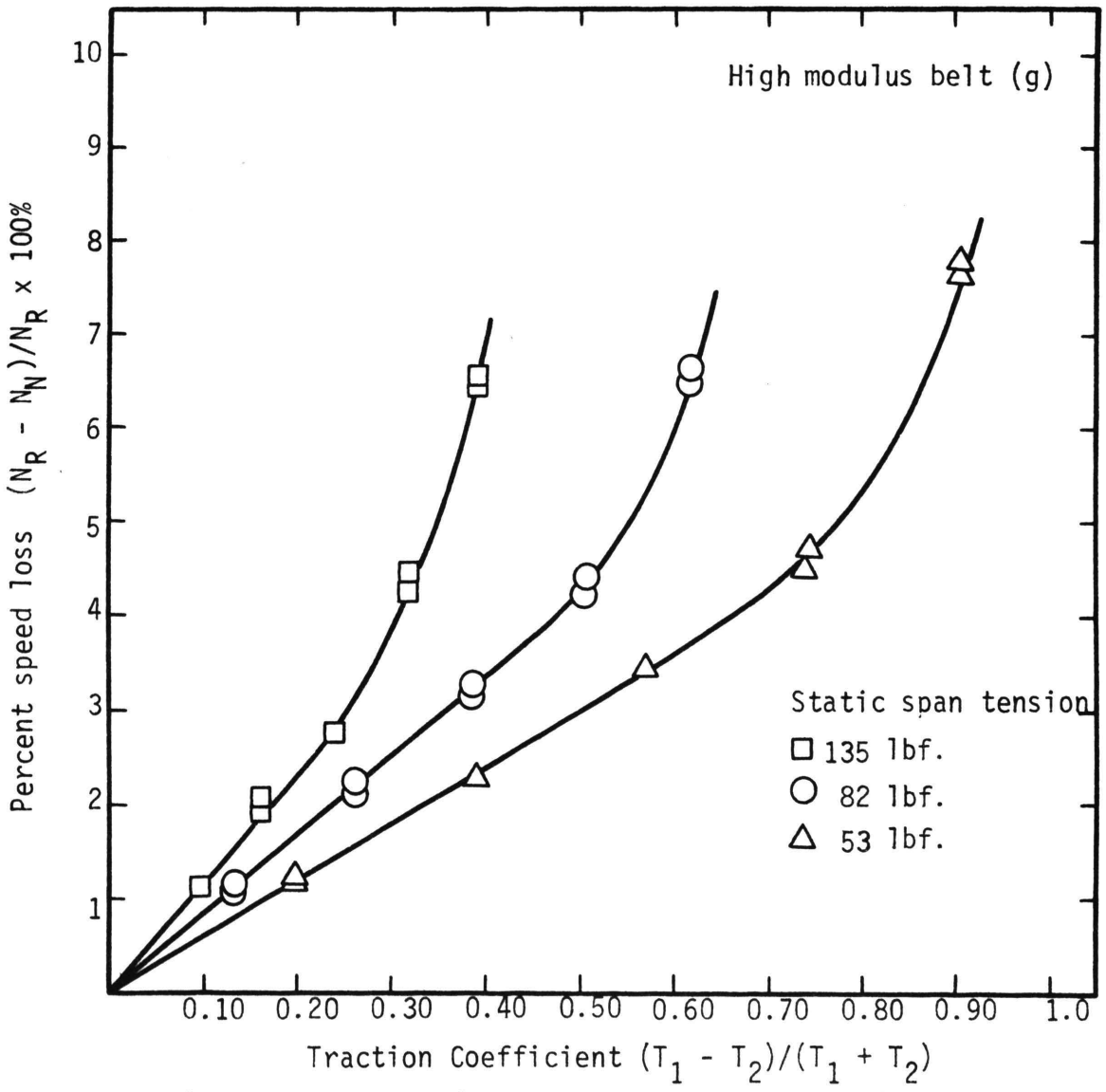

Figure 6.18. Speed Loss Versus Traction Coefficient for 2, 2 1/4 inch diameter pulleys near 1200 RPM

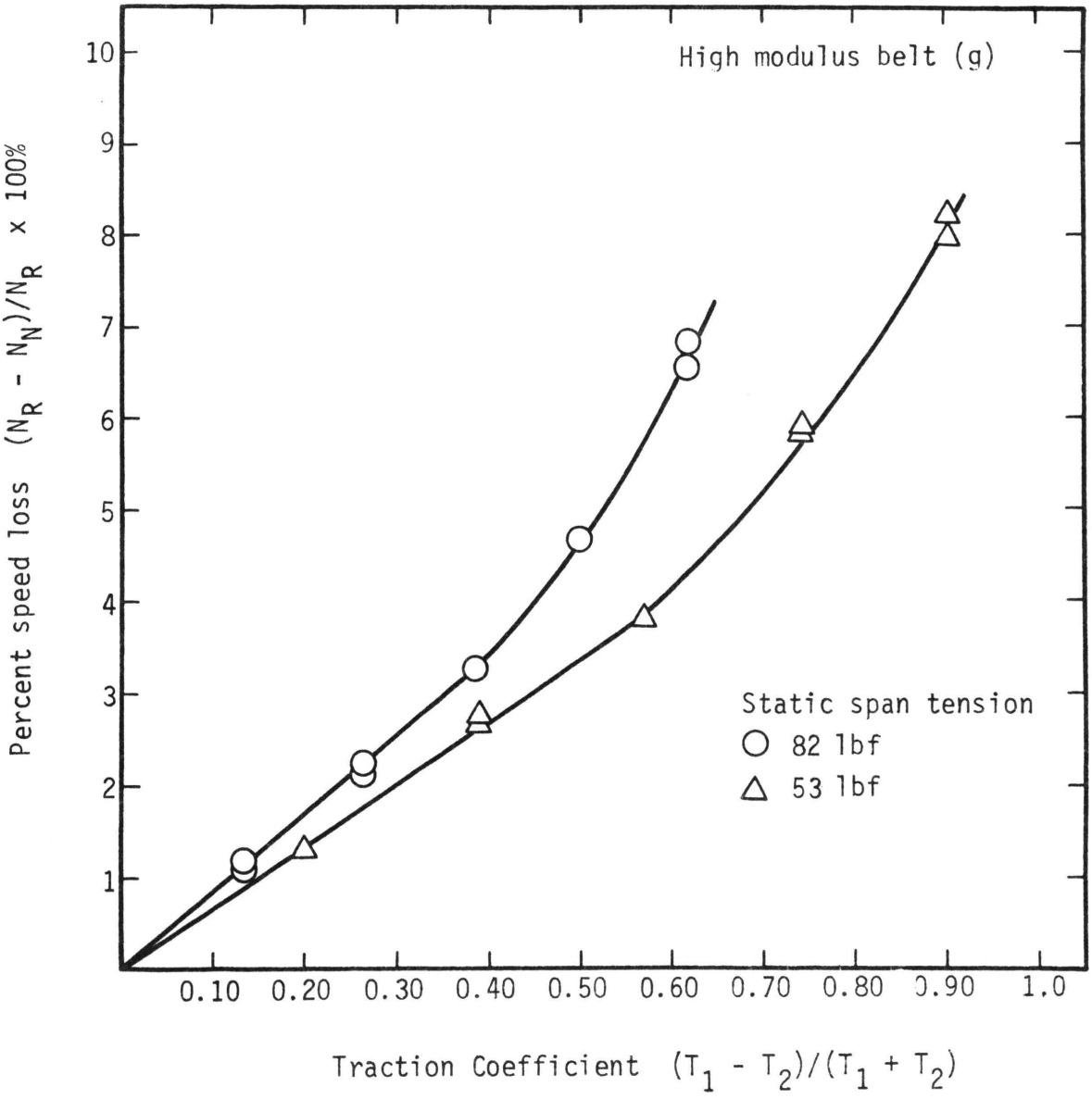

Figure 6.19. Speed Loss Versus Traction Coefficient for 2, 2 1/4 inch diameter pulleys near 2400 RPM

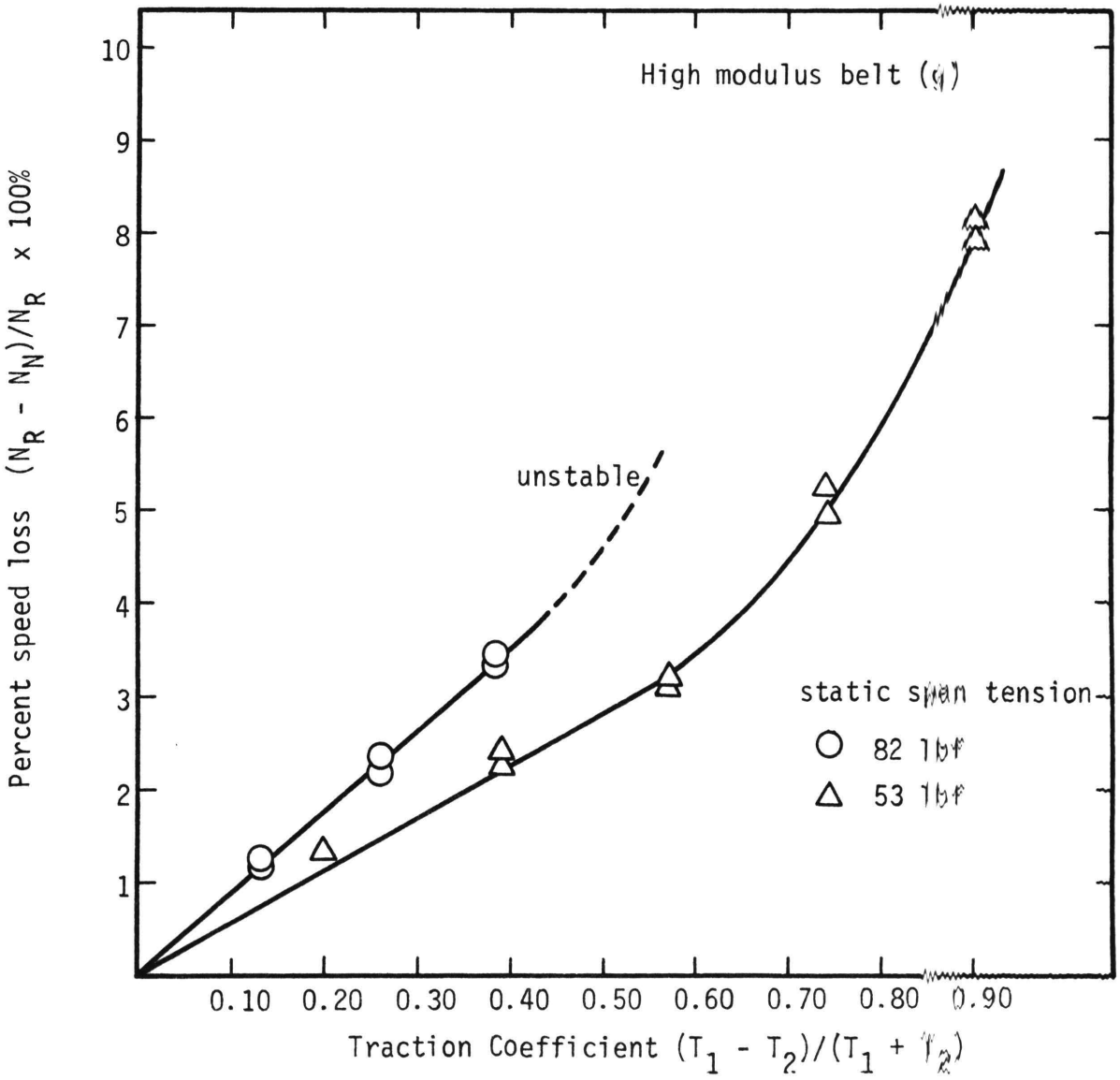

Figure 6.20. Speed Loss Versus Traction Coefficient for 2, 2 1/4 inch diameter pulleys near 3600 RPM

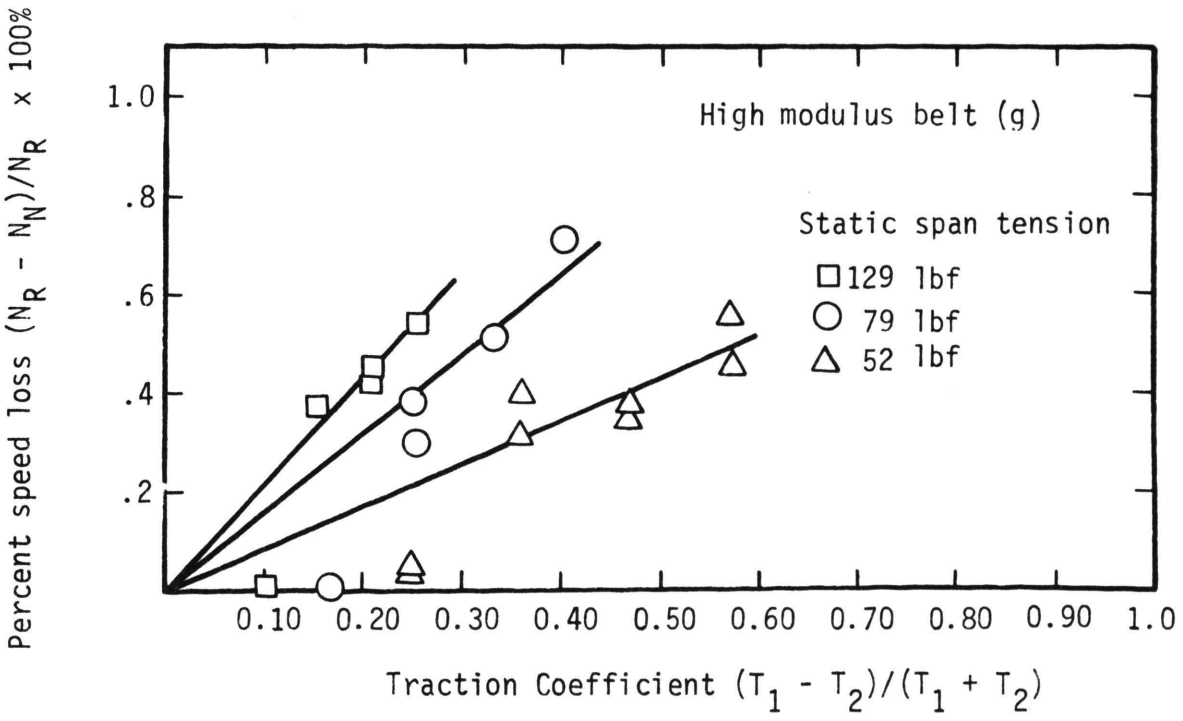

Figure 6.21. Speed Loss Versus Traction Coefficient for 2, 3 1/2 inch diameter pulleys near 1200 RPM

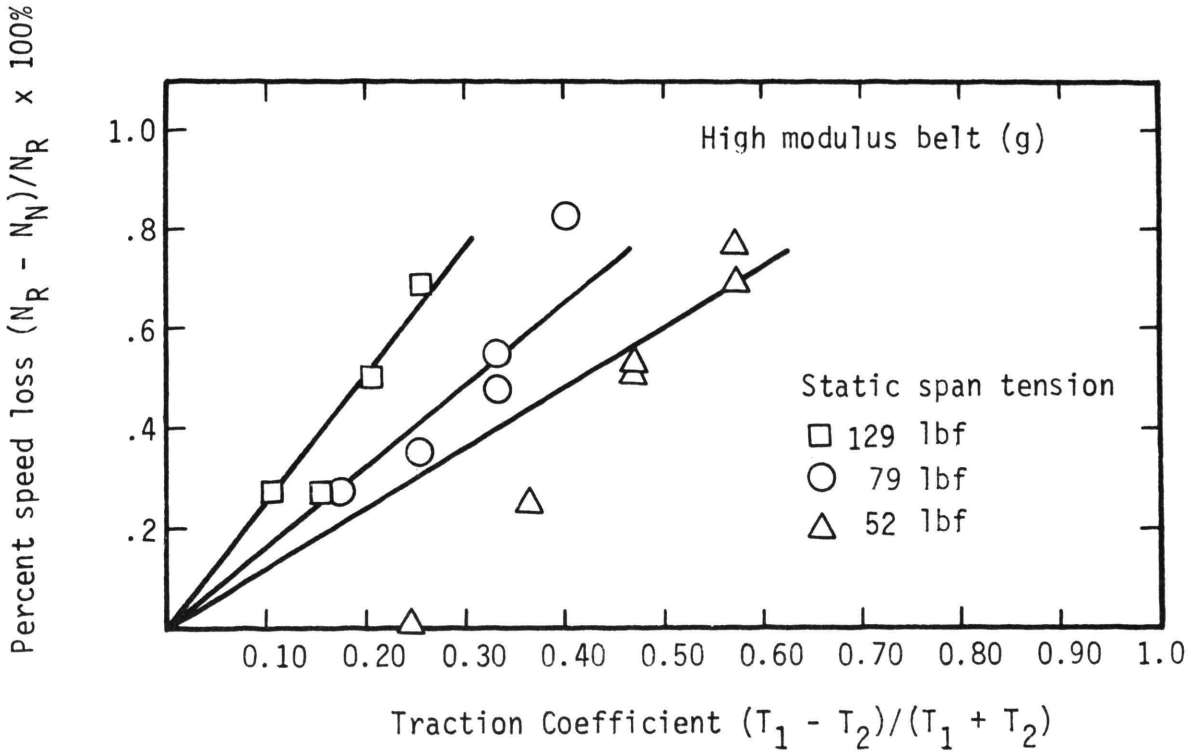

Figure 6.22. Speed Loss Versus Traction Coefficient for 2, 3 1/2 inch diameter pulleys near 2400 RPM

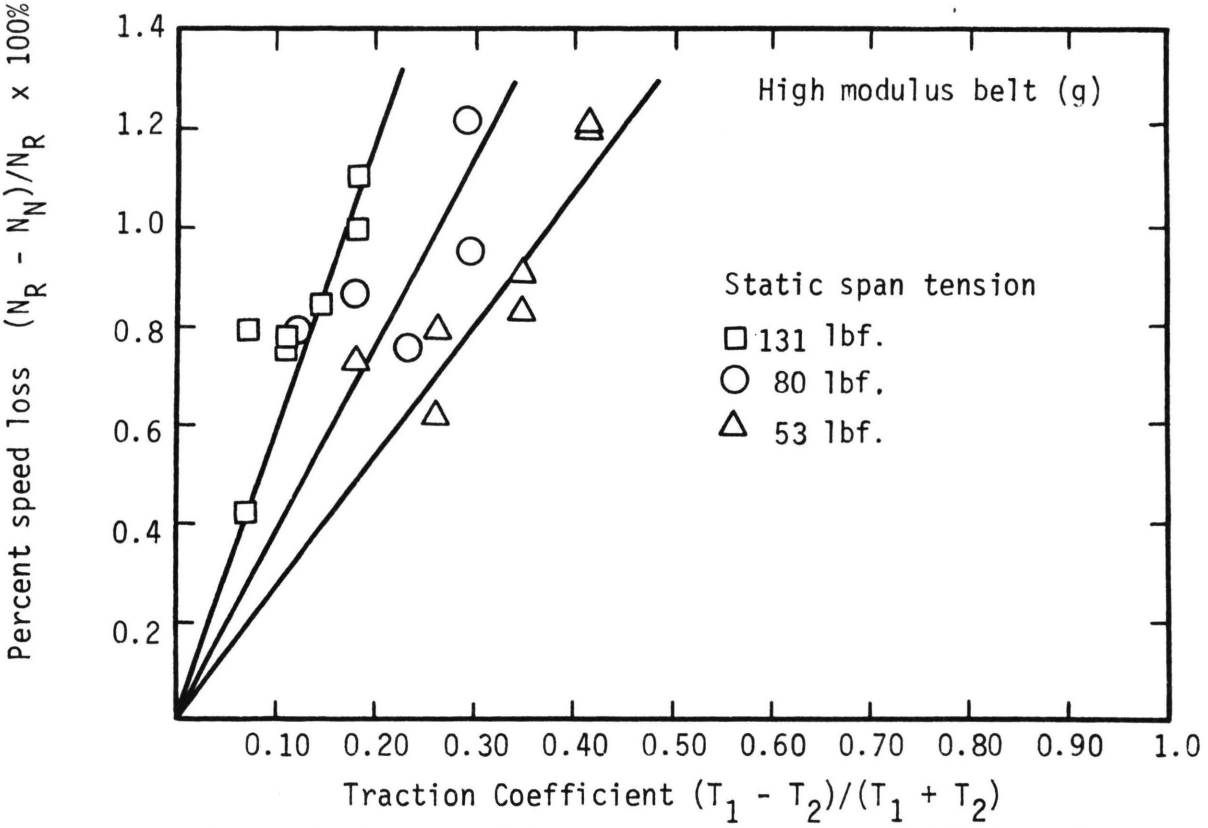

Figure 6.23. Speed Loss Versus Traction Coefficient for 2, 4 3/4 inch diameter pulleys near 1200 RPM

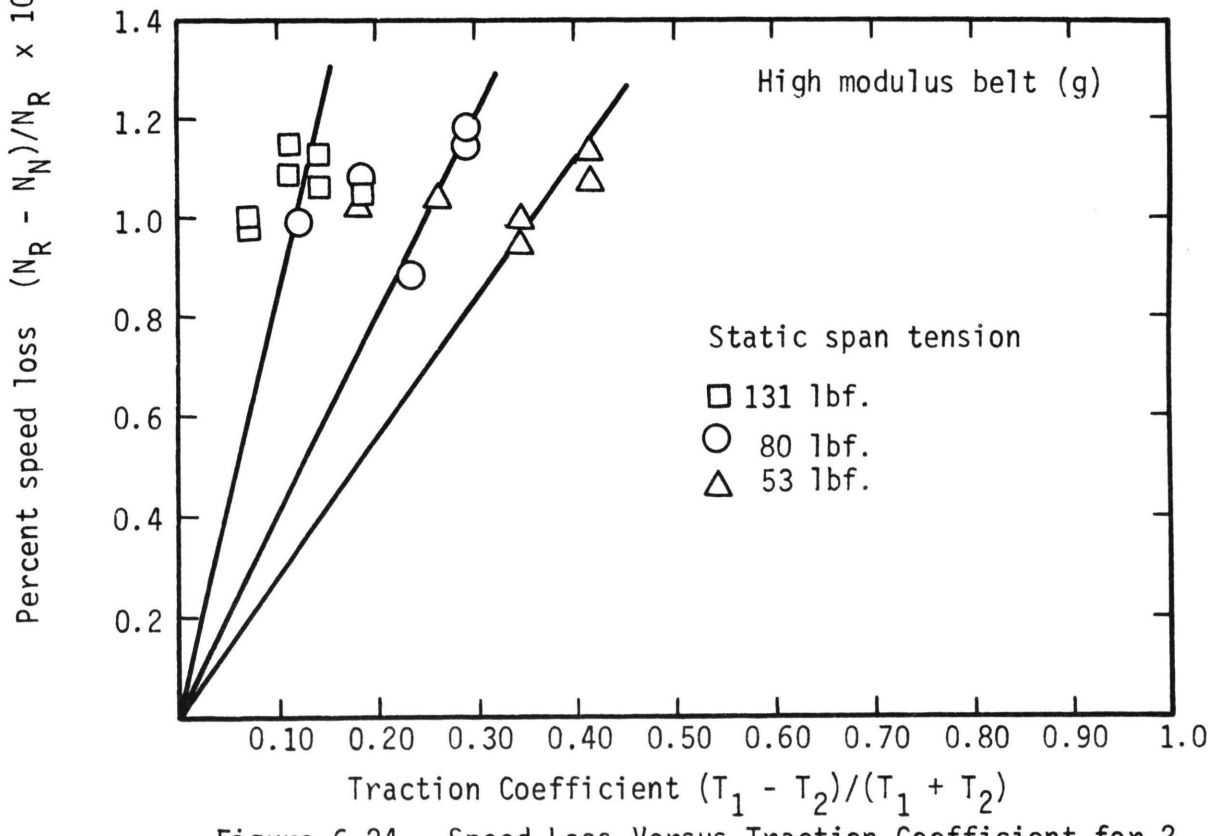

Figure 6.24. Speed Loss Versus Traction Coefficient for 2, 4 3/4 inch diameter pulleys near 2400 RPM

with the data from the 2 1/4 inch pulley in Figures 6.19 through 6.21.

The drive employing 2 1/4 inch pulleys generated enough heat at 2,400 and 3,600 RPM with $T_1 + T_2 = 250$ pounds to visibly destroy itself in a short length of time. The tests run with the 3 1/2 and 4 3/4 inch diameter pulleys did not allow belt burn-up for the speeds and preloads tested, but a determination of the steady state operating temperature field on the slip versus traction coefficient curve would be useful in defining the design acceptability of these drives.

Gross properties such as percent power loss, traction coefficient, and steady state operating temperature are important considerations in belt drive design because of their relation to fatigue. The stress analysis conducted in this study has shown that increasing the torque load on an automotive v-belt drive leads to a small percentage increase in maximum cord tensile stress. Because belt life is significantly altered by increasing the torque load on a given drive; slip, shear, and heat generation must be considered as fatigue factors along with increasing load stress in order to justify the faster fatigue rate. Since this report does not consider belt fatigue quantitatively, the main purposes of the slip tests were to identify the magnitude of belt power losses and to determine the linear design range of slip versus traction coefficient for the drive situations tested in the stress analysis.

VII. CONCLUSIONS

An objective of this study has been the determination of the relative magnitudes of stress components in automotive range v-belt drives. The experimental system allowed the calculation of dynamic free span tensions. Bending stresses were successfully determined by a static test, and centrifugal stresses were calculated for the drive situations employed. Load stress variation over driver and driven pulleys caused by torque transmission was determined from a digital simulation program after unsuccessful attempts at experimental measurement. Superposition of all stress components permitted the determination of the stress cycle in an automotive belt drive. The insight gained from the attempt to photograph strains in a dynamic torque loaded drive has led to a set of recommendations for a more precise photography system which may be capable of measuring load strains in future work.

The investigation of static bending stress supports several implications for belt drive design. The graphs of neutral axis elevation versus preload show that the neutral axis elevation varies with pulley size, preload, and from the center of the belt to the edge. No single constant value for the neutral axis elevation in a given belt design may, therefore, be justified in design equations. It has also been shown that neutral axis elevation depends on cord material, belt configuration, and relative cord size as illustrated by the differing results for the two types of belts tested during this investigation. Absolute compressive stresses and strains were shown to exist in the belt cord layer due to the combination of

compressive bending stresses and tensile load stresses below the elevation of zero stress. The cyclic cord stress variation might then be required to include tensile and compressive cycling because a single cord strand wraps from one stress condition to the other. For preloads yielding the sum of the tight and slack side tensions between 80 and 280 pounds and for the 2 1/4, 3 1/2, and 4 3/4 inch diameter pulleys used, maximum bending stress in the belt cords has been shown to be at least several times the preload tensile stress. The high time rate of rise and fall of bending stress as the belt enters and leaves the pulley sheave has been established. Common fatigue analysis would probably multiply maximum bending stress by a factor of two to account for the faster fatigue rate of a material subjected to suddenly applied stresses.

The slip versus traction coefficient data illustrated the high efficiency of the v-belt as a flexible driving link and allowed determination of suitable design ranges of torque and preload for the drive situations tested. It was also recognized from these tests that steady state operation temperature of a belt system was dependent on slip, traction coefficient, pulley size and preload.

The Hornung analysis of belt tension variation due to torque loading was used to complete the stress analysis because of the failure to obtain these data experimentally. The magnitude of cord stress variation due to the change from slack side tension to tight side tension is small compared to maximum bending stress, but the shear, creep, slip, and heat generation processes which accompany load stress transfer are known to have a noticeable effect on belt

life. The problem of measuring the load stress variations in the axial and tangential directions around the v-pulleys in a high speed torque loaded drive is therefore still important.

It is the purpose of these conclusions, then, to examine an improvement of the photographic technique for determining belt deformation in the dynamic state. Success has already been achieved in stopping high-speed belt motion by the use of a strobe, flash delay and photoelectric pickoff. The strobe possessed two more flash ranges of lower intensity but shorter duration than the one used for the photographs of Figure 6.12, allowing for as little as 0.8 microsecond exposure time if faster drive speeds were employed.

Suggestions for improving the measurement capability from photographic negatives are as follows. A macro lens on the 35 millimeter camera should be used instead of the extension tubes used in this experiment. The macro lens provides life size images on the 35 millimeter film negatives at focal lengths of 6 or 7 inches compared to the approximately 2 1/2 inch lens to object distance used with the extension tubes. The greater focal length offered by the macro lens should minimize the effect of small changes in radial ride position on image sharpness. In order to improve the quality of the photographic negatives and reduce grain size, a finer grain film such as Kodak Plus-X rather than Kodak Tri-X should be used. The quality of the photographic target on the belt must also be improved. In the present study, the lines scribed on the belt were nearly 0.01 inches wide. In order to measure maximum strains of less than one percent, a very thin or sharp edged line must be

constructed on the belt. The use of a thin coating of a compatibly elastic material over the cord layer would provide a smooth surface on which the marks could be made. If possible, a grid instead of axial lines should be laid out on this surface to provide the capability of measuring shear and load stress variation in the axial direction. The use of a cathometer to measure distances as small as 0.01 millimeter on an enlarged projection of a photographic negative still appears to be the most precise method of extracting data presently at our disposal.

The improvements recommended here should be applied first to statically loaded belts to demonstrate their feasibility before a new test system is built. In order to provide several data points for a tight side to slack side tension difference of fifty pounds, a ten pound tension change should provide a repeatably measurable strain change in the static test. For a common low modulus belt modulus belt where M_t = 20,000 $lb/\frac{in.}{in.}$, this requirement constitutes the measurement of 0.0005 inches per inch to a prescribed accuracy.

If the photographic measurement technique is established by the static tests, the new dynamic test rig should employ a camera mount which would allow for precision measurement of the focal length. This feature is necessary because inadvertent change in focal length may cause significant change in the size of the photographed belt image as compared to the small strains being measured. An attempt should also be made to get a precision scale in each photograph to allow for calibration of each photograph with respect to the same reference. In the new test setup, the camera should be isolated from vibrations in

the rotating equipment. The new apparatus for dynamic testing of v-belts should be built as a three pulley drive with driven shafts mounted on fixed centers. The smaller contact angles of a three pulley drive and the fixed centers condition would more closely simulate automotive v-belt systems.

Still another possibility for measuring load strain effects in the event that the photographic system does not function may be strain gages. Strain may be measured from a ballasted gage system on a slowly rotating torque loaded drive and recorded on an oscilloscope or strip chart recorder. This technique has already been used by others, but extensive data for automotive size belts and pulleys in three pulley drive geometry is not available. Again, strain variation across the belt in the axial direction could be made from center and edge mounted gages. Water brakes might be used for absorption in this system to provide the necessary torques at low speeds.

Finally, this report has established experimental measurements of span stress, bending stress and power loss in automotive scale v-belt drives. Unsuccessful attempts were made at measuring load and shear stress variation due to torque transmission. The analysis was completed with analytical determination of these quantities. Experience gained from unsuccessful experimentation has, however, prompted the discussion of the feasibility of accomplishing these tasks in future experimental work.

BIBLIOGRAPHY

1. Bowen, Gary Lynn. "Dynamic Properties of V-Belt Material," Ohio State University Thesis, 1972.

2. Chin-Heng, Chen. "Dynamic Properties of V-Belts," Ohio State University Thesis, 1971.

3. Doyle, Eric and Hornung, Kenneth G. "Lateral Vibration of V-Belts," A.S.M.E. Paper no. 69-VIBR-29, Presented at the American Society of Mechanical Engineers Vibrations Conference, Philadelphia, Pennsylvania, March 1969.

4. Garrett, Peter L. "Equations for Computing Creep in V-Belt Drives," Product Engineering, (March 4, 1961), 86-89.

5. Gerbert, B. G. "Tensile Stress Distribution in the Cord of V-Belts," A.S.M.E. Paper no. 73-DE-D, Contributed by the Design Engineering Division of the American Society of Mechanical Engineers for publication in the Journal of Engineering for Industry, (November 1972).

6. Gerbert, B. G. "Pressure Distribution and Belt Deformation in V-Belt Drives," Transactions of Machine Elements Division, Lund Technical University, Lund, Sweden, (1973).

7. Hornung, Kenneth G. "Factors Influencing the Fatigue Characteristics of Rubber Textile Machine Elements," Ohio State University Dissertation, 1959.

8. Hornung, Kenneth G., Marco, S. M., and Starkey, W. L. "Tension Variations in V-Belts Applied to Locked Center Drives," A.S.M.E. Paper no. 60-WA-307, Presented at the Winter Annual Meeting of the American Society of Mechanical Engineers, New York, New York, November 1960.

9. Johnson, C. O. and Hornung, Kenneth G. "Reliability Predictions for V-Belts," not published.

10. Marco, S. M., Starkey, W. L., and Hornung, K. G. "A Quantitative Investigation of the Factors Which Influence Fatigue Life of a V-Belt," Transactions of the American Society of Mechanical Engineers, Journal of Engineering for Industry, Series B, Volume 82, no. 1, (February 1960), 47-59.

11. Martynov, V. K. "Tangential Deformations in V-Belt Transmissions," Russian Engineering Journal, Volume 50, no. 3, (1970), 44-49.

12. Meyer, Alton H, Jr. "Photographic Study of V-Belt Motion Over a V-Pulley," Ohio State University Thesis, 1961.

13. Pronin, B. A.; and Shmelev, A. N. "Losses in a Wide Belt Variable Speed Drive," Russian Engineering Journal, Volume 50, no. 9, (1970), 45-47.

14. Shade, W. N. "Heat Generation and Dissipation in a V-Belt Drive," Ohio State University Thesis, (1970).

15. Upchurch, James Michael "Heat Generation and Dissipation in Loaded V-Belt Drive," Ohio State University Thesis, 1971.

16. Virabov, R. V. "Constant Mass Conditions in Belt Drives," Russian Engineering Journal, Volume 47, no. 4, (1967), 28-31.

17. Virabov, R. V. "The Traction Properties of Belt Drives," Russian Engineering Journal, Volume 46, no. 7, (1966), 40-44.

18. Worley, William Spencer. "Design of V-Belt Drives for Mass Produced Machines," Product Engineering, (September 1953), 154-162.

VITA

John Mark Wiesehan was born on December 27, 1951 in St. Louis, Missouri. He received his primary and secondary education near St. Louis and was graduated from Lindbergh High School in June 1969. He was enrolled at the University of Missouri-Rolla in September 1969 and received his Bachelor of Science degree in Mechanical Engineering in July 1972.

Since August, 1972, he has attended the Graduate School of the University of Missouri-Rolla and has been supported by teaching and research assistantships for the period from August, 1972 through August, 1973.

APPENDIX A

EQUIPMENT LIST

a. Variable Speed D.C. Motor

General Electric Shunt Wound D.C. Cradled Dynamometer Motor, model 5T206A5, type B, 7 1/2 H.P. maximum at 250 volts, 1800-4000 RPM.

b. Balance Scale

Toledo Balance Scale, style 0861, no. 704483, range 0-100 pounds with 0.1 pound increments.

c. Alternators

Prestolite Alternator, model ALB-52025, output 12 volts, 60 amps, negative ground.

d. Field Voltage Supply

Heathkit Battery Eliminator, model BE-5, output 0-15 volts D.C.

e. Electronic Force Transducer

Daytronic Force Transducer, model 152-A, range 0-1000 pounds.

f. Electronic Force Transducer Indicator

Daytronic Transducer Amplifier Indicator, model 300D with type 70 Differential Transformer Input Module.

g. High Modulus Test Belt

Dayco Die-cut V-belt; A cross section; top width, 0.497 inches; pitch length, 48.5 inches; v-angle, 36^{o}; tangential belt modulus, M_t = 53,308 lbf./(in./in.) at 0.1 and 1 inches/second shaft separation; axial modulus, M_a = 1545 (lbf./in.)/(in./in.); outside cord diameter, D = 0.037 inches; cord cross sectional area, A = 0.00066 $in.^2$; single cord modulus, M_{cord} = 4250 lbf./(in./in.); ultimate cord strength, 196

pounds (for a single cord); cord material, Dupont Kevlar with temperature insensitive modulus.

h. Low Modulus Test Belt

Dayco Die-cut V-belt; a cross section; top width, 0.497 inches; pitch length, 48.5 inches; v-angle, 36^{o}; tangential belt modulus, M_t = 17,037 lbf./(in./in.) at 0.1 and 1 inches/second shaft separation and M_t = 24,961 lbf./(in./in.) at 10 inches/second shaft separation; axial modulus M_a = 1404 (lbf./in.)/(in./in.); diameter D = 0.055 inches; cord cross-sectional area, A = 0.00173 $in.^2$; single cord modulus, M_{cord} = 1860 lbf./(in./in.); ultimate cord strength, 169 pounds (for a single cord); cord material, Dupont Dacron Polyester.

i. 2 1/4 Inch Diameter Test Pulley

Pitch diameter, 2.250 inches; sheave width, 0.500 inches; v-angle, 36^{o}; bore diameter, 0.75 inches; key width, 1/4 inch; key depth, 1/8 inch.

j. 3 1/2 Inch Diameter Test Pulley

Pitch diameter, 3.500 inches; sheave width 0.500 inches; v-angle, 36^{o}; bore diameter, 0.75 inches; key width, 1/4 inch; key depth, 1/8 inch.

k. 4 3/4 Inch Diameter Test Pulley

Pitch diameter, 4.750 inches; sheave width, 0.500 inches; v-angle, 36^{o}; bore diameter, 0.75 inches; key width, 1/4 inch; key depth, 1/8 inch.

l. Strain Gages

Micro Measurements Strain Gage; type EA-06-250BG-120; Resistance, 120 ohms; gage factor at 75^{o} F, 2.095; polymide encapsulated.

m. Strain Indicator

Budd Protable Strain Indicator; Model P-350; used in quarter bridge circuit; strain range, 0-50,000 microstrain; gage factor, 0-10.

n. 35 mm Camera

Miranda 35 mm camera, lens no. 4561918 Auto Miranda; f = 5 cm, 1:1.9; extension tubes, 1/4 inch + 1/2 inch + 1 1/2 inches.

o. Flash Delay

General Radio Flash Delay; type 1531-P2; 105-125v; 50-60 c.; Delay Range, 0.0001-0.8 seconds; output pulse, 13v; minimum input pulse, 0.3 volts.

p. Photoelectric Pickoff

General Radio Photoelectric Pickoff; type 1536-A, operating rate, approx 2500 pulses/second; power required 20-28 volts D.C., 40 ma.

q. Electronic Stroboscope

General Radio Strobotac Electronic Stroboscope; 110-25000 flashes per minute; type 1531-AB; flash duration at 1/3 peak intensity, approximately 0.8, 1.2, and 3 μ seconds for high, medium and low speed ranges respectively; power required 105-125 or 210-250v, 50-400 Hz, 35 w.

r. Cathometer Microscope

W. G. Pye and Co. Ltd. Cathometer Microscope, Serial no. 100597.

s. Magnetic Pickoff

Airpax zero velocity Magnetic Proximity Pickoff; model 14-0001; utilizes Hall Effect; 2 logic states, 0 volts D.C. and 5 volts D.C.

t. Electronic Counter

General Radio Electronic Counter; type 1191-B; time interval, 0.1 μ seconds to 10^9 seconds; accuracy to ±1 count ±time base accuracy.

u. Hand Tachometer

Hasler Hand Tachometer; catalog no. 9961; speed range, 0-10000 RPM; accuracy, ±0.25%.

v. Overhead Projector

3-M Brand Overhead Projector.